Article:
Jain, S., Onuaguluchi, O., Banthia, N. et al. (2025) Advancements in immobilization of cesium and strontium radionuclides in cementitious wasteforms—a review. Journal of the American Ceramic Society, 108 (1). e20131. ISSN: 0002-7820

https://doi.org/10.1111/jace.20131

Advancements in immobilization of cesium and strontium radionuclides in cementitious wasteforms – a Review

Shubham Jain[a,b *], Obinna Onuaguluchi[b], Nemkumar Banthia[b], Tom Troczynski[a]

[a]*Materials Engineering Department, University of British Columbia, Vancouver, Canada*

[b]*Civil Engineering Department, University of British Columbia, Vancouver, Canada*

Corresponding author –*Shubham Jain, Materials and Civil Engineering Department, University of British Columbia, Vancouver, Canada.

Email: shubham.jain@alumni.ubc.ca / shubham.jain.cer10@iitbhu.ac.in

Postal address: 6250 applied science lane, Vancouver, BC Canada V6T 1Z4

Contact number: +91 8828308946

Abstract

The safe and secure encapsulation or immobilization of nuclear waste, particularly low to intermediate-level waste (accounting for ~97% of the total volume of nuclear waste), has been a significant concern. Consequently, numerous studies have been conducted on various materials such as Ordinary Portland Cement (OPC)-based, bitumen, and ceramics for the purpose of waste encapsulation/immobilization. However, these studies generally offer a broad overview of materials performance without focusing on specific radioisotopes of concern. Cesium (Cs) and strontium (Sr) are important radioactive nuclides to consider for encapsulation, but the existing studies on immobilizing these elements are fragmented and lack a comprehensive understanding. This critical review article offers a thorough qualitative and quantitative analysis to uncover the primary trends/knowledge gaps within the field. It comprehensively delves into waste classifications/management and leaching assessments, followed by an exploration of the immobilization performance and durability issues of various traditional and advanced cementitious materials including low-temperature chemically bonded ceramics like alkali-activated matrices (AAM) and Mg-K phosphates for the immobilization of Cs and Sr. Further, the review article provides fresh insights and perspectives, including recommendations for improvements, novel technologies, and future trends in this domain.

Keywords: Immobilization; Encapsulation; Hazardous Nuclear Waste; Alkali-Activated Materials; Geopolymers; Ordinary Portland Cement; Leaching

1. Introduction

1.1 Nuclear power as a future energy source

Nuclear energy is gaining prominence as a crucial alternative for electricity generation, offering clean, reliable, and affordable power on a large scale, with low carbon emissions. According to the World Nuclear Association (WNA), nuclear power is considered low-carbon, and **Figure 1** illustrates the average life-cycle carbon dioxide-equivalent emissions, revealing significantly lower emissions from nuclear power plants (~12 gCO_2 released per equivalent of 1 kWh generated) compared to fossil fuels, coal, and natural gas (~2280 gCO_2-eq/kWh) [1,2]. Currently, 440 power reactors contribute around 10% of the world's electricity, positioning nuclear power as the second-largest source of low-carbon power globally (28% in 2019) [3]. Nuclear energy is also utilized in over 220 research reactors across 50 countries, supporting various applications such as medical/industrial isotope production and training [4]. Depending on the cost and performance of low-carbon technologies, nuclear electricity is estimated to potentially avoid ~3.3 to 9 Gt CO_2/year by 2050 [5].

In addition to its low carbon footprint, nuclear power has one of the lowest external costs concerning damage to human health and the environment, not reflected in electricity prices. Uranium resources are globally accessible and contribute only a small fraction to the overall cost of nuclear electricity. The energy density of nuclear fuel allows for the production of 50 MWh of electricity per 1 kg of nuclear fuel, significantly surpassing the efficiency of fossil fuels, oil, and coal (where only 0.003−0.004 MWh of electricity is produced per kg of fuel) [2,6].

Even though nuclear technology has significant advantages, its wide acceptance is closely associated with warranting benign and sustainable approaches to the disposal of harmful

radioactive waste. Therefore, effective waste management systems are implemented to prevent any adverse effects on ecological systems.

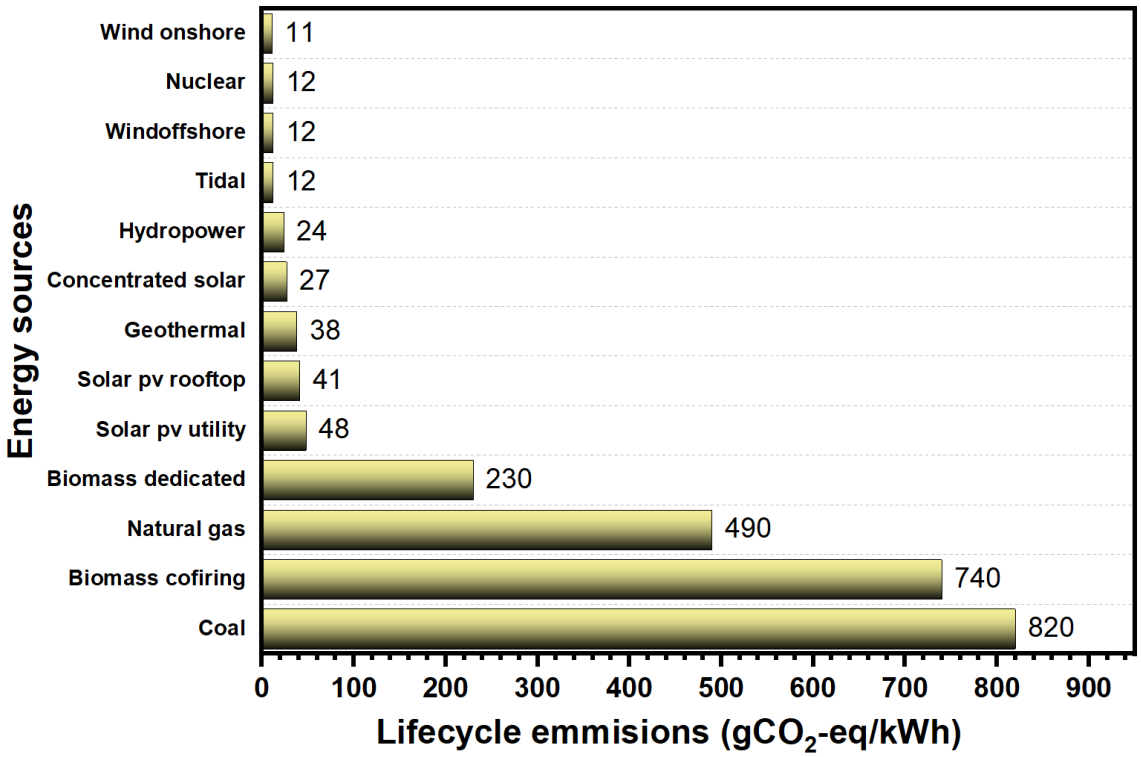

Figure 1: Average life-cycle carbon dioxide-equivalent emissions from different electricity generators [1].

1.2 Radioactive nuclear waste classifications and management

Radioactive nuclear waste is described as any material that is either inherently radioactive or contaminated by radioactivity and has no further use. However, for legal and regulatory purposes, radioactive waste is defined as waste that comprises or is contaminated with radionuclides at activities or concentrations exceeding clearance levels as established by the regulatory body [7].

1.2.1 Radioactive waste classifications

Classification of waste is critical from a safety and process consideration point of view. Generally, essential parameters considered for classification include physical, chemical, radiological,

biological properties, and the origin of the waste. The classification system is implemented to ease the management of a particular waste type. Different management options are implemented based on the radioactivity levels in the waste and the shielding requirements. In terms of the activity limits, radioactive wastes are classified by IAEA based on two parameters: radionuclide half-life and radioactivity content, as shown in **Figure 2**. The detailed characteristics of these classes are listed in **Table 1** [8].

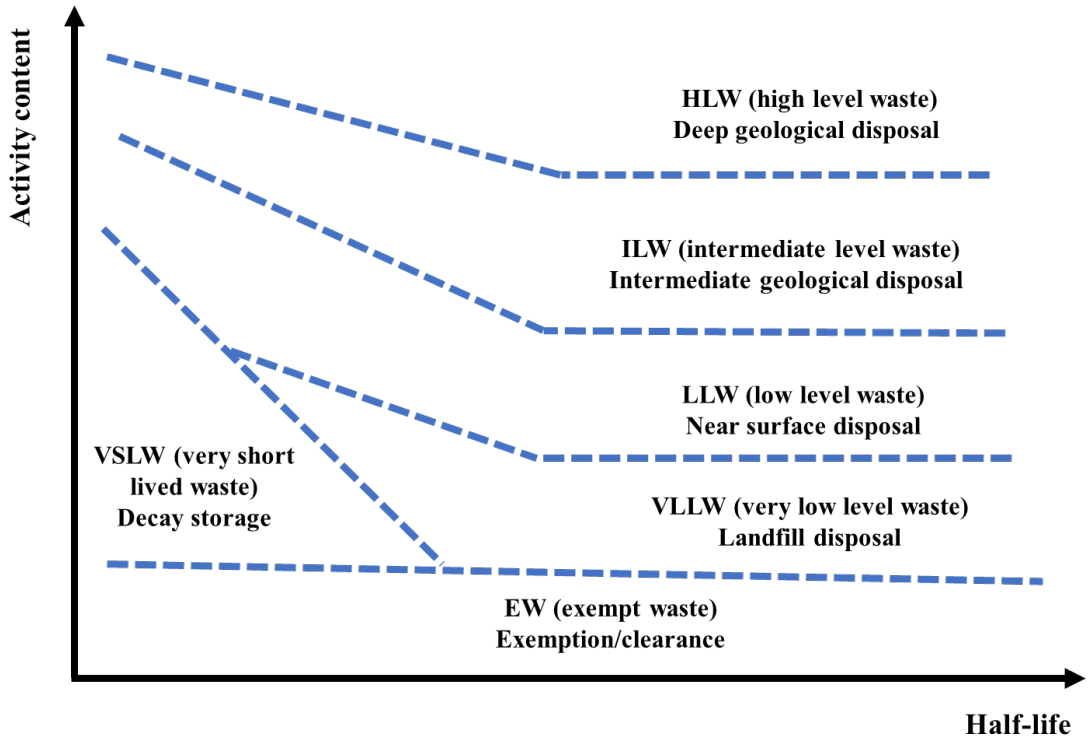

Figure 2: Conceptual illustration of the waste classification scheme by International Atomic Energy (IAEA) Agency Safety Standards [8].

Table 1
Radioactive waste classifications as per the International Atomic Energy Agency (IAEA) [8].

Waste classes	Acronyms	General characteristics
High-level waste	HLW	The activity concentration is high enough to generate significant quantities of heat or wastes with large amounts of long-lived radionuclides.
Intermediate-level waste	ILW	Long-lived radionuclide concentrations, in particular, alpha-emitting radionuclides that will not decay to a level of activity concentration acceptable for near-surface disposal during an institutional control period. ILW also includes waste that needs no provision, or only limited provision, for heat dissipation during storage and disposal.
Low-level waste	LLW	Activity levels are above clearance levels with a limited amount of long-lived radionuclides. It requires robust isolation and containment for periods of up to a few hundred years and is suitable for disposal in engineered near-surface facilities.
Very low-level waste	VLLW	Activity levels are above clearance levels but do not need a high level of containment; it can be disposed of near-surface with limited regulatory control. The concentrations of longer-lived radionuclides are very limited.
Very short-lived waste	VSLW	Waste that can be stored for decay over a limited period of up to a few years and subsequently cleared from regulatory control.
Exempt waste	EW	Waste meets the criteria for clearance, exemption, or exclusion from regulatory control for radiation protection purposes.

Figure 3 shows the volume and the level of radioactivity distribution in % of nuclear waste among the waste classes. HLW accounts for only ~ 3% of the total volume of nuclear waste but 95% of the total radioactivity of produced waste. On the other hand, ILW accounts for ~7% of the total volume and comprises 4% of the radioactivity in nuclear waste. The vast majority ~90% of the

volume is comprised of LLW but contains only 1% of the radioactivity [9]. In addition, a few examples of exemption levels for waste nuclides (regulated by IAEA) and essential characteristics such as half-life and specific activities are shown in **Table 2** [10].

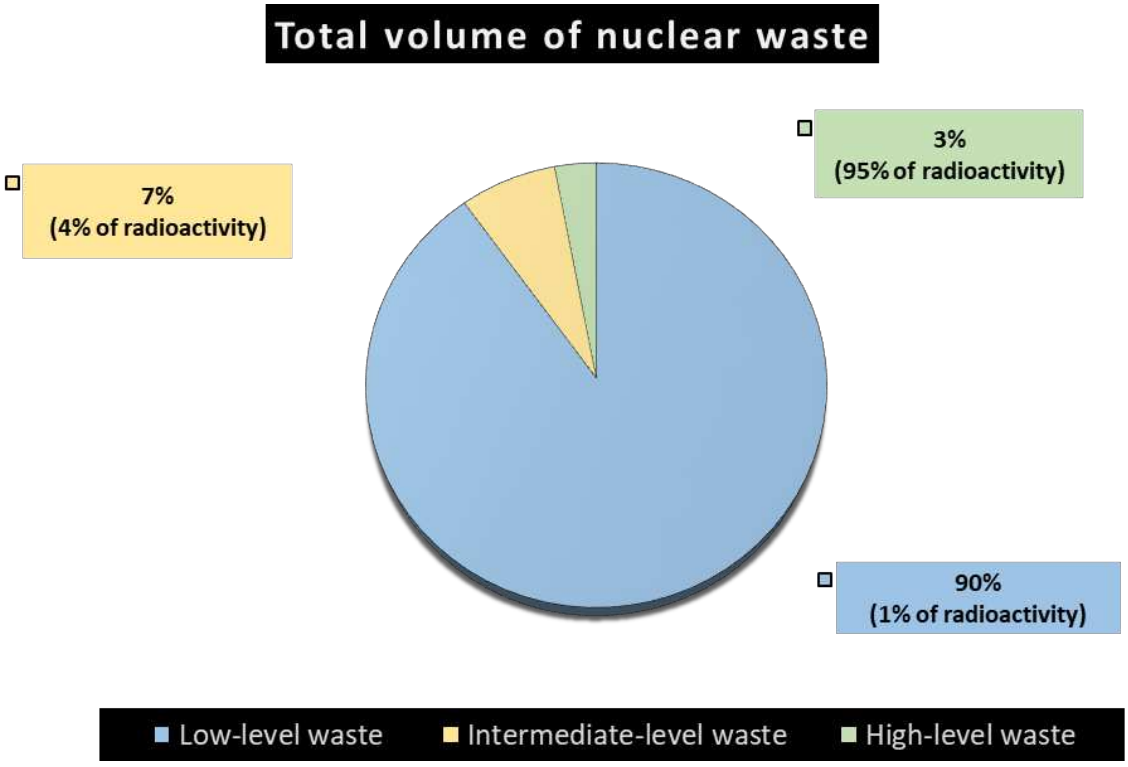

Figure 3: Volume and radioactivity distribution (%) of nuclear waste classes based on the World Nuclear Association [9,11].

Table 2

Examples of radionuclide characteristics, exempt activity concentrations, and exempt activities as per the International Atomic Energy Agency (IAEA) [10].

Nuclide	Half-life (Years)	Specific activity (Ci/g)	Exempt activity concentration (Bq/g)	Exempt activity (Bq)
^{134}Cs	2.06	1294	10	10^4
^{135}Cs	3.0×10^6	1.15×10^{-3}	10^4	10^7
^{137}Cs	30.17	86.98	10	10^4
^{90}Sr	28.50	136.40	10^2	10^4
^{60}Co	5.27	1131	10	10^5
^{232}Th	1.4×10^{10}	1.09×10^{-7}	1	10^3
^{235}U	7.0×10^8	2.16×10^{-6}	10	10^4
^{238}U	4.5×10^9	3.36×10^{-7}	10	10^4

1.2.2 Radioactive waste management

Waste management is an essential practice for public acceptance of nuclear energy from a safety point of view. According to international and national regulations, the wastes require effective management to diminish the quantities of radioactive contaminants to the level that warrants the safe discharge of the decontaminated liquid to the environment and the safe disposal of the concentrated radionuclides [12]. The general main steps of radioactive waste management, which are implemented worldwide, are shown in **Figure 4**. These steps mainly include waste characterization, treatment, conditioning, storage, disposal, and surveillance/monitoring [13].

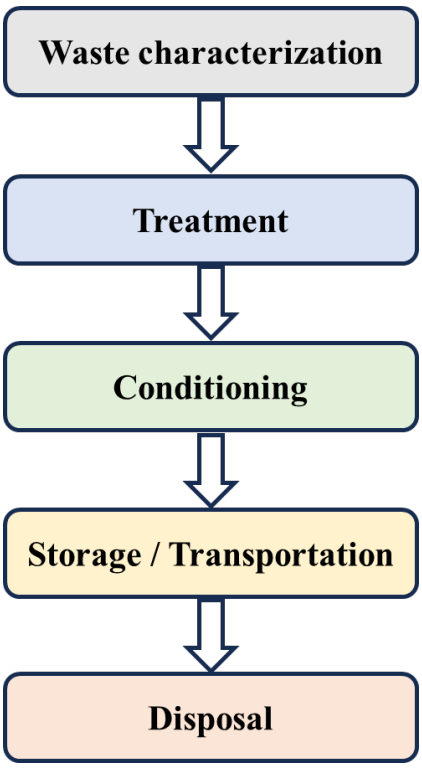

Figure 4: General schematic of radioactive waste management [13].

A summary of the radioactive waste management steps as per IAEA (2007) [13] are described as follows:

"Characterization*: Characterization of waste is essential at every stage of waste management, especially at the beginning. It involves determining the physical, chemical, and radiological properties of the waste. Characterization is helpful to segregate radioactive materials for exemption, reuse, and disposal methods or to warrant compliance of waste packages with requirements for storage and disposal.*

Treatment*: This step includes operations to alter the characteristics of the radioactive waste, which are intended to improve safety or the economy. A variety of treatments may result in an appropriate wasteform for disposal. However, the treated waste requires further conditioning either by solidification, immobilization, or encapsulation in most cases.*

Conditioning*: This step incorporates processes such as cementation, polymerization, bituminization, or vitrification that produce a waste package suitable for handling, transportation, storage, and disposal.*

Storage*: This step comprises preserving the radioactive waste to ensure retrievability. Further, confinement, isolation, ecological protection, and monitoring are looked after during the storage period.*

Transportation*: Careful conveyance of radioactive waste in specially designed packages.*

Disposal: *Emplacement of waste in a suitable facility without the intention of retrieval."*

Among the management steps mentioned above, waste conditioning is a crucial step, especially for low and intermediate-level liquid wastes (LILW). Radioactive liquid wastes, in general, consist mainly of metal hydroxide sludge containing most of the fission products and actinides, plus a supernatant solution of mainly Na hydroxide, Na nitrate, Na nitrite, and Na aluminate, together with soluble fission products such as Cs and Tc [4]. Conditioning transmutes the waste into a form suitable for handling, transport, storage, and disposal by immobilization of radioactive waste. Immobilization ensures the safe embedding of radioactive waste into a matrix, preventing the leakage of radionuclides into the environment. Conditioning, in general, is achieved by incorporating the wastes in solid monoliths of low dispersibility. Standard immobilization methods for LILW include cementation, polymerization, geopolymerization or bituminization, and vitrification for HLW.

1.3 Major radionuclides of concern in the nuclear waste

1.3.1 Cesium

Cesium (Cs) is a soft, silvery white-gray metal that occurs in nature as non-radioactive ^{133}Cs and consists of 55 protons and 78 neutrons [14]. Pollucite is the rare naturally occurring mineral source that yields the greatest quantity of Cs. There are 11 major radioactive isotopes of Cs, and only three (^{134}Cs, ^{135}Cs, and ^{137}Cs) have relatively long half-lives (about 2 to 2 million years) and high specific activity (0.0012−1300 Ci/g), **Table 2**. These three isotopes of Cs are produced by nuclear fission and decay by emitting beta particles.

The isotopes of Cs, especially ^{137}Cs (yield ~6 %) and ^{135}Cs (yield ~7 %), are among the most common heavy fission products by the nuclear fission of ^{235}U and other fissionable materials in nuclear reactors or nuclear weapons [15]. ^{137}Cs is typically considered the isotope of paramount concern as per the Department of Energy (DOE) since it is produced with a relatively high yield of ~6 % (i.e., 6 atoms are produced per 100 fissions). In addition, the half-life of ^{137}Cs is ~30 years, and it emits one to two high-energy beta particles, **Figure 5** [16]. Most of the ^{137}Cs decay results in a 662 keV gamma-ray emission with a half-life of ~2.6 minutes to form the decay product ^{137}Ba. Due to this decay product, Cs becomes an external hazard (i.e., a hazard without intake in the body).

When compared to ^{137}Cs, ^{135}Cs, and ^{134}Cs are less concerning due to their radiological decay characteristics. ^{135}Cs has a long half-life of ~2.3 million years and low specific activity (0.0012 Ci/g). Therefore, the low decay energy combined with the slow decay rate contributes to the low hazards of ^{135}Cs. On the other hand, ^{134}Cs have a half-life of only ~2.1 years, and it decay by emitting a beta particle; hence, ^{134}Cs decay rapidly to cause any long-term adverse impact on the environment.

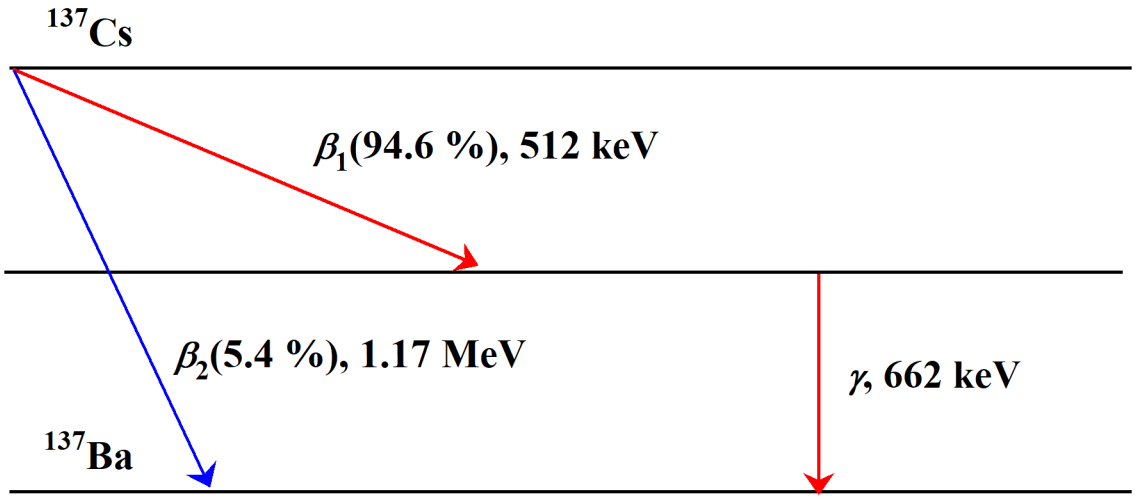

Figure 5: Schematic illustration of ^{137}Cs decay [16].

In terms of chemical characteristics [14], Cs belongs to the alkali metals group and has an oxidation state of +1 (including isotopes). Due to the highly electropositive nature of Cs, it is very reactive toward water. Cesium salts and most cesium compounds are generally water-soluble and reactive; for example, cesium hydroxide (CsOH) has a very high-water solubility of 4 kg/L at 15 °C and can chemically attack even stainless steel. CsOH is also gauged as the most likely cesium compound released from the nuclear reactor in a severe accident. Additionally, due to its high solubility in the water released from the nuclear reactor, it is expected to persist in the environment and have long-term contamination hazards.

The intake of Cs can cause a severe internal health hazard for humans or animals. The primary health concern is the increased prospect of inducing cancer due to beta and gamma radiation. Besides hazards of internal exposures, there is a considerable risk from the external gamma rays exposure.

Due to the properties such as decay by high-energy pathways, high water solubility, and chemical reactivity, which may lead to perilous health hazards and long-term adverse impacts on the environment [4], effective conditioning of ILLW containing cesium is paramount.

1.3.2 Strontium

Strontium (Sr) with an atomic number of 38 is an s-block, alkaline-earth metal located in group 2 and period 5 of the periodic table. Sr is a soft and chemically reactive metal that is water-soluble. The stable and naturally occurring Sr has four isotopes; ^{84}Sr, ^{86}Sr, ^{87}Sr, and ^{88}Sr, with the ubiquitous ^{88}Sr making up approximately 83% [17,18]. Conversely, a number of radioactive Sr isotopes ranging from ^{73}Sr to ^{107}Sr have also been reported by few studies [19–21]. The data in **Table 3** indicates that ^{82}Sr and ^{85}Sr decay to half of the atomic nuclei within 25-65 days by simultaneously absorbing an orbiting electron in the nucleus, followed by the conversion of a proton to a neutron and the emission of a neutrino/gamma-ray. For the ^{89}Sr and ^{90}Sr isotopes, they typically undergo a beta-minus decay process whereby a neutron is converted to a proton, an electron, and an electron antineutrino. ^{90}Sr is typically produced with a yield of about 5-6% from the radioactive fission of uranium, plutonium, and other nuclear species in reactors [22]. The ^{90}Sr can also be retrieved from spent nuclear fuel (SNF) and high-level liquid waste (HLLW) solutions.

Similar to ^{137}Cs, ^{90}Sr could be released to the environment through nuclear weapon discharge, nuclear accidents, disposed SNF, and other radioactive wastes [23,24]. However, the big challenge is curtailing ^{90}Sr contamination at disposal sites. Although, **Table 3** shows that ^{90}Sr has the longest half-life of 28.9 years, thus with the low activity level, it will take more than 200 years to decay to less than 1% of the atomic nuclei. Therefore, given the number of years it will take to decay to a negligible and non-toxic level; ^{90}Sr is classified as a High-level Waste (HLW). Moreover, the decay of ^{90}Sr to the short-lived yttrium (^{90}Y) is also problematic due to the emission of high-energy

beta radiation. Indeed, beta radiation from ^{90}Sr decay is quite hazardous, with the capacity to cause cancer and inflict bone-related terminal illnesses in humans [25].

Table 3
Properties of several radioactive isotopes of strontium (adapted from Semenishchev and Voronina, 2020 [21]).

Isotope	Decay mode	Half-life	Beta-plus/ beta-minus energy (MeV)	Gamma energy (keV)
^{82}Sr	Electron capture	25.3 days	No beta-plus	No gamma
^{85}Sr	Electron capture	64.8 days	No beta-plus	514
^{89}Sr	Beta-minus	50.5 days	1.5	909
^{90}Sr	Beta-minus	28.9 years	0.5	No gamma

1.4 Release of nuclides from cementitious materials

Generally, most of the radioactive waste solids are multi-phase heterogeneous materials, and mass transfer in these materials is complicated by several processes that typically happen simultaneously. Transport is possible along many paths such as inside crystal lattices, along crystal grain boundaries, intraparticle voids or through pore volumes, along pore surfaces, and through interparticle voids [26]. In addition, chemical reactions, dissolution-precipitation, vaporization-condensation, and other mechanisms may affect the transport, and the mobile species may be migrating in either the solid, liquid, or gaseous state. Hence, an "effective diffusivity", D_e, is defined in the mass transport equation when transport is known to be happening simultaneously via several mechanisms [27]. The effective diffusivity must be determined experimentally, and the question of the particular (or dominating) diffusion mechanism is difficult to elaborate. The assumption made in such a case is that the transport equation including D_e can adequately represent the system from the practical point of view.

Commonly, the release of nuclides from cementitious materials is dominated by diffusion [28,29]. However, if other mechanisms such as corrosion, erosion, and dissolution are important, their control is discernible only after extended leaching periods [28]. Consequently, determining the effective diffusion coefficient for the species of interest provides a meaningful way to predict the maximum release from the wasteform to water.

There are various leaching test standards, with the most commonly used being ANSI/ANS-16.1 and ASTM C1308-21. Additionally, other leach testing protocols have been applied in various published studies, including ASTM C1285, the Chinese GB7023 standard, and the French National Radioactive Waste Management Agency - ANDRA standard. However, a one-to-one comparison and interpretation of test results obtained from different leaching test methods is quite challenging. This difficulty arises from the wide variation in experimental conditions such as specimen size/geometry, liquid/solid ratio, leaching solution replacement frequency, and differences in pH levels and temperature conditions. A summary of the most common leaching test standards, ANSI/ANS-16.1 and ASTM C1308-21, is discussed in the subsequent sections.

1.4.1 American Nuclear Society (ANS) 16.1 standard for the leaching test

Several leaching tests assume bulk diffusion, as described by Fick's law, as the primary mechanism governing the release of nuclides [30,31]. One widely used procedure is the ANSI/ANS 16.1 standard, which provides a uniform method to assess material suitability as a wasteform for targeted low/intermediate-level waste elements, quantified by the leachability index (*LX*) [28].

The ANSI/ANS 16.1 test involves immersing a monolith specimen in deionized water, replacing the leachant at designated intervals over 5 days, and extendable up to 90 days. The test protocol includes maintaining a constant ratio of leachant volume to the specimen's exposed surface area

and monitoring the cumulative leaching fractions (CFL). The resulting data are used to calculate the effective diffusivity (D_e) and subsequently, the leachability index (LX).

The effective diffusivity (D_e) of the solid monolith wasteform is derived from Fick's second law, the solutions to which depend on specimen shape and size as outlined in ANSI/ANS 16.1 [28]. If < 20% (CFL < 0.2) of a leachable species is leached from a uniform, regularly shaped solid, its leaching behavior (if diffusion controlled) approximates that of a semi-infinite medium. Under these conditions the mass-transport equations permit the calculation of an "effective diffusivity" by **Eq. 1**. If more than 20% of a leachable species has been leached by the time, t, the effective diffusivity can only be calculated from a shape specific solution of the mass transport equations.

$$\boldsymbol{D_e = \pi \left[\frac{a_n/A_0}{(\Delta t)_n}\right]^2 \times \left[\frac{V}{S}\right]^2 \times t_m} \qquad \textbf{Eq. 1}$$

Where a_n = quantity of a nuclide (Cs) released from the specimen during the leaching interval n in g, A_0 = total quantity of a given contaminant (Cs) in the specimen at the beginning of the first leaching interval (i.e., after the initial 30-s rinse) in g, V = volume of the specimen (cm^3), S = exposed surface area of the specimen (cm^2), $(\Delta t)_n$ = duration of the n^{th} leaching period in seconds, t_m = leaching time representing the "mean time" of the n^{th} leaching interval.

The leachability index (LX), **Eq. 2**, is a material parameter defined by the ANS 16.1 standard as "an index value related to the leaching characteristics of solidified waste materials". It is used to quantify the ability of a wasteform to impede the release of hazardous components when the material comes in contact with water. As specified in the standard, the U.S. Nuclear Regulatory Commission requires that LX meets a minimum acceptable value of 6.0 [28].

$$LX = \frac{1}{n}\sum_{i=1}^{n}\left[log\left(\frac{1}{D_e}\right)\right]_i \qquad \textbf{Eq. 2}$$

1.4.2 IAEA (ASTM C1308-21) standard for the leaching test

Similar to the ANS 16.1 standard, the IAEA semi-dynamic leach test standard [32] provides a systematic approach for evaluating how radionuclides are released from solidified materials. It suggests experimental conditions to ensure accurate results, and to determine immobilization performance of wasteforms. The standard can aid in identifying whether the release is due to mass transport (like diffusion), surface dissolution, or a combination of both. When mass diffusion is the main release mechanism, the test results could be used to calculate diffusion coefficients, which are essential for mathematical models that rely on diffusion. For surface dissolution, the kinetic dissolution rate could be calculated, crucial for dissolution-based modeling.

In cases where both mechanisms are involved, the test method recommends the assessment of effective diffusion coefficient values, which contributes to an improved understanding of the release mechanism. Further, elevated temperatures could be used in the tests to accelerate the leaching process and determine the temperature range where the release mechanism is consistent. Results obtained at higher temperatures could be used to estimate releases at lower temperatures over longer periods.

The test procedure involves immersing a well-defined specimen (typically a cylinder or a cuboid) in a specified volume of leachant (the leachant volume used for each interval is 10x the surface area of the specimen), with a complete replacement of the leachant at regular one-day intervals. Subsequently, the concentration of a specific element is measured in the recovered solution after each interval. The test results are then utilized to calculate the incremental fraction leached (*IFL*) and cumulative fraction leached (*CFL*). These values are subsequently subjected to analysis to

ascertain whether an analytical model can effectively describe the release process. In summary, this method proves highly valuable for comprehending the release of substances from materials, especially within the context of waste forms and the assessment of long-term contamination.

2. Immobilization of radionuclides in Portland Cement-based composite systems

For immobilization of LILW (predominantly liquid waste), the primary viable conditioning technology that is commercially prevalent is cementation [33,34]. The most widely used cement-based inert "binders" are Ordinary Portland cement (OPC), cement–polymer composites, and alternative binding systems [4,34]. These materials are low-cost (OPC cost in USA was approximately between $120 to $130 per metric ton in 2018-2023) and readily available [35]. For several decades now, OPC has been used for the immobilization of nuclear waste in most developed countries of the world. This is traceable to its high resistance to ion transport, its solubility-limiting high alkalinity, and the availability of a huge surface area in cement hydrates that is conducive for the sorption/ion exchange of radionuclides. The proposed binding mechanisms in the cement systems include the precipitation of metal ions into the alkaline matrix as an oxide, incorporation of metal ions into hydrated cement materials, or adsorption of metal ions onto the cement surface [36]. Previous studies [37–39] have shown that economical and readily available OPC composites are very good at acting as either a physical barrier or chemical binder of radionuclides and other toxic metals. Besides its low cost and availability, cement is also tolerant of both solid and liquid low/intermediate-level radioactive waste (LILW) with highly varying characteristics. It remains stable and durable over time, thereby minimizing risks to the general public (IAEA-TECDOC-1397 [40]; IAEA-TECDOC-1701 [41]). In a recent review, Tyupina et al. [42] provided a comprehensive summary of the applications of Portland cement composites either as a matrix/buffer material or as a lining/backfilling material component in nuclear waste disposal facilities.

2.1 Immobilization of cesium in traditional cementitious materials

Immobilization studies of Cs ions in traditional cementitious materials have reported rather poor performance, with relatively high effective diffusivity D_e = 10^{-7} to 10^{-9} cm^2/s in short and long-term leaching assessments [12,43]. **Table 4** summarizes the reported effective diffusivities (D_e) in cement-based systems for Cs immobilization. The immobilization mechanism in OPC-based systems is mainly based on the precipitation of the corresponding hydroxides due to the highly alkaline pore solution (physical immobilization) [44]. However, this mechanism is ineffective for highly soluble Cs (solubility of CsOH in water ~4 kg/L at 15 °C), which also results in high effective diffusivity [45]. Therefore, to improve the immobilization of Cs ions, zeolites or pozzolanic additives have been attempted. However, incorporating zeolite-A in Portland cement or alternative cement variants showed only a minor improvement in the immobilization $D_e \sim 5.7\times10^{-8}$ cm^2/s [12]. Furthermore, fly ash belite cement blended with Na-P1 zeolite showed improved immobilization with $D_e = 10^{-9}$ cm^2/s, about two orders of magnitude lower than the OPC [38]. Nevertheless, the reported D_e values are not considered effective for Cs immobilization or appropriate for disposal, as per Environment Canada guidelines [46]. The use of unconventional high-performance cementitious materials, such as Sulphoaluminate cement (SAC) as explored by Xu et al. [47], demonstrated enhanced Cs immobilization, yielding a D_e value of 8.8×10^{-10} cm^2/s. The Cs immobilization mechanism was attributed to physical fixation and mineralogical immobilization in the SAC matrix. Additionally, Pyo et al. [48] conducted a study on Magnesium Potassium Phosphate (MPP) cement, revealing improved Cs immobilization with a resulting D_e value of 3.5×10^{-12} cm^2/s. However, the study did not provide a comprehensive explanation of the Cs immobilization mechanism within the MPP systems.

Table 4
Summary of the reported effective diffusivities (D_e) in cement-based systems for Cs immobilization.

Material	Test method	Effective diffusion coefficient D_e (cm^2/s)	Reference
PC - type I	ANSI/ANS 16.1	1.2×10^{-7}	Jang et al. [49]
PC - type I	IAEA	2.4 to 4.7×10^{-8}	Papadokostaki et al. [43]
PC - type I	IAEA	4.6×10^{-7}	El-Kamash et al. [12]
PC - type I	ANSI/ANS 16.1	1.7×10^{-7}	Guerrero et al. [45]
PC - type IV		5.9×10^{-8}	
PC – type V (water/cement = 0.35)	Not applicable	1.1×10^{-8}	Johnston and Wilmot et al. [50]
PC – type V (water/cement = 0.25)		2.6×10^{-9}	
PC blended with zeolite A	IAEA	5.7×10^{-8}	El-Kamash et al. [12]
Cementitious wasteforms	Not applicable	10^{-12} to 10^{-10}	Ojovan et al. [51]
FABC	ANSI/ANS 16.1	2.2×10^{-7}	Goñi et al. [44]
FABC with Na-P1 zeolite		2.8×10^{-9}	
PC (w/c = 0.4)	China GB/T 7023	3.6×10^{-9}	Xu et al. [47]
SAC		8.8×10^{-10}	
PC (w/c = 0.4)	ANS 16.1	2.7×10^{-8}	Goo et al. [52]
MPP cement	ANS 16.1	3.5×10^{-12}	Pyo et al. [48]

Where PC: Portland cement; FA = Fly ash; FABC = Fly ash belite cement; SAC = Sulphoaluminate cement; MPP = Magnesium Potassium Phosphate.

2.2 Immobilization of strontium in traditional cementitious materials

Table 5 summarizes the reported effective diffusivities (D_e) in various cement-based systems for Sr immobilization. Investigations into the immobilization of Sr in conventional OPC-based systems (for the water-to-cement w/c ratios between 0.35-0.5) have revealed moderate results, showing variable effective diffusivity (D_e) values ranging from 10^{-8} to 10^{-11} cm^2/s in both short and long-term leaching evaluations. The addition of zeolite-A in Portland cement resulted in about a 31% reduction in Sr effective diffusivity [12]. Atkins and Glasser et al. [37] were of the opinion that the immobilization of Sr occurs either through sorption by cement hydrates or through high pH-induced precipitation. Evans et al. [38] suggested that whereas low levels of Sr could be immobilized in C_4AF, C_3A, and C-S-H, C-S-H of low Ca:Si ratio, AFt and C_3AH_6 were more effective in immobilizing Sr. This was partly confirmed in the study by Ke et al. [39] which showed that the immobilization of radionuclides occurred mainly in C-S-H gel, ettringite and calcium carbonate phases. The expansive micropores and surface area make the C-S-H conducive for the adsorption of radionuclides [53]. A specific surface area of approximately 700 m^2/g has been reported for the C-S-H [54].

The utilization of unconventional high-performance cementitious materials, such as Sulphoaluminate cement (SAC) as investigated by Xu et al. [44], exhibited a one order of magnitude reduction in the effective diffusivity of Sr immobilization relative to an OPC matrix, yielding a D_e value of 7.9×10^{-12} cm^2/s. A recent study on the use of Wollastonite-based brushite cement by Jdaini et al. [55] demonstrated effective Sr immobilization, reporting a D_e value of 4.4×10^{-15} cm^2/s. Further, Pyo et al. [45] conducted a study on Magnesium Potassium Phosphate (MPP) cement, revealing significantly improved Sr immobilization with a resulting D_e value of 2.8×10^{-17} cm^2/s after 90 days of test duration.

Table 5

Summary of the reported effective diffusivities (D_e) in cement-based systems for Sr immobilization.

Material	Test method	Effective diffusion coefficient D_e (cm^2/s)	Reference
PC - type I (w/c = 0.5)	ANSI/ANS 16.1	3.3×10^{-10}	Jang et al. [49]
PC	IAEA	1.4×10^{-13}	Barnes et al. [56]
PC (w/c = 0.4)	IAEA	1.4 to 4.5×10^{-12}	Matsuzuru and Ito [57]
PC (w/c = 0.35)	IAEA	5.4×10^{-8}	El-Kamash et al. [12]
PC blended with zeolite A (w/c = 0.35)		3.7×10^{-8}	
PC (w/c = 0.4)	ANS 16.1	7.6×10^{-11}	Goo et al. [52]
MPP cement	ANSI/ANS 16.1	2.8×10^{-17}	Pyo et al. [48]
PC (w/c = 0.4)	China GB/T 7023	7.3×10^{-11}	Xu et al. [44]
SAC (w/c = 0.4)		7.9×10^{-12}	
Wollastonite-based brushite cement Cement (L/S = 1.25)	ANSI/ANS 16.1	4.4×10^{-15}	Jdaini et al. [55]

Where PC: Portland cement; SAC = Sulphoaluminate cement; MPP = Magnesium Potassium Phosphate.

2.3 Limitations of Ordinary Portland cement (OPC)-based materials as a conditioning matrix for cesium and strontium

In addition to the poor immobilization of soluble radionuclides, OPC has further limitations concerning the adverse impact on the environment, acid corrosion resistance, thermal stability, freeze-thaw behavior, and radiolytic hydrogen [4,58,59]. The cement sector is the second-largest

global industrial CO_2 emitter; it is estimated that OPC production alone contributes 1.35 billion tons of GHG emissions each year [60]. Approximately 1 ton of CO_2 is generated to produce 1 ton of cement [61]. The two main processes that emit CO_2 in cement production are the kiln calcination of limestone ($CaCO_3$ + heat → $CaO + CO_2$) and the combustion of fossil fuels for heating [62]. Global cement production is increasing every year and in recent years, cement-related CO_2 emissions have reached ~10% of total global CO_2 emissions, **Figure 6**. Therefore, there is an urgent need to minimize CO_2 emissions from the cement industries, which could be achieved either by producing clinker-free cement or by partially/completely replacing OPC with supplementary cementitious materials.

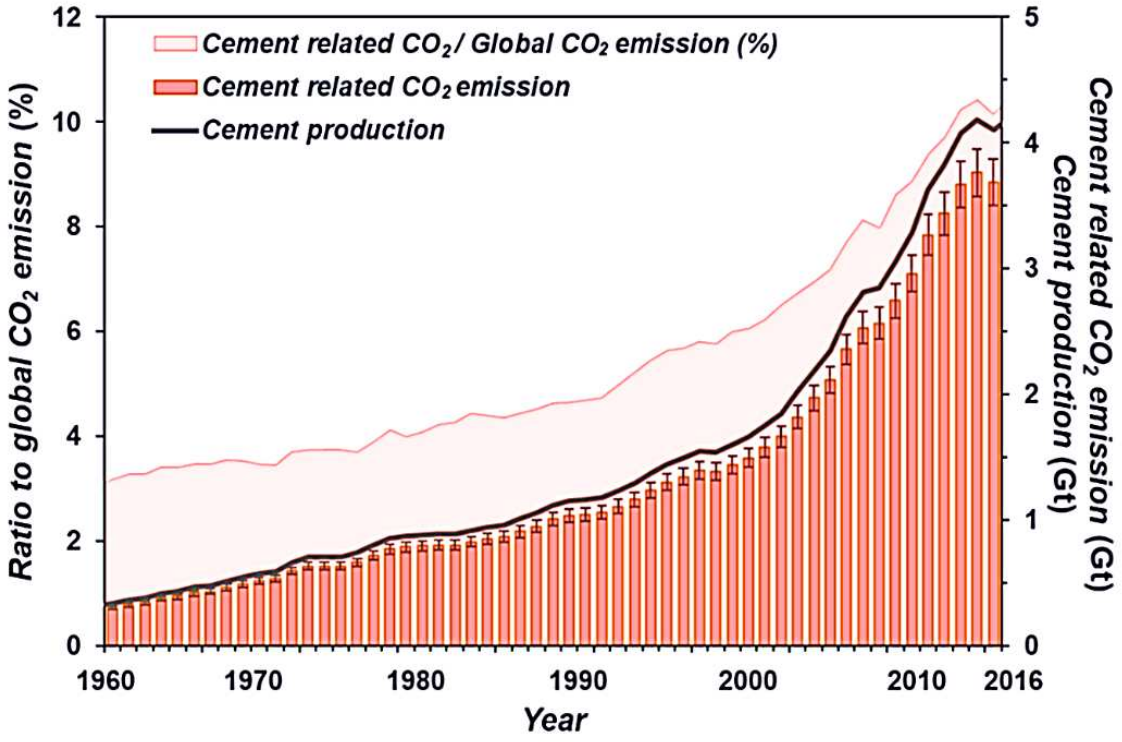

Figure 6: CO_2 emissions related to cement production and its ratio to total CO_2 emissions [62].

Significant weight loss was determined in the OPC matrix after the acid corrosion test [58,63]; for example, immersion of OPC in acetic acid and sodium acetate-based buffer solution (pH = 3.6) for

60 days resulted in ~25% matrix mass being lost within the first 20 days and the mass loss continued with the remaining immersion time [58]. The deterioration or mass loss in OPC in an acidic environment is caused by the dissolution of calcium hydroxide crystals and the decalcification of calcium silicate hydrate gels. The dissolution of these phases under an acidic environment typically leads to increased porosity and enlarged capillary pores, noticeably unfavorable for Cs immobilization [64]. In addition, exothermic geological activities and nuclear disintegration of radioactive waste could increase the temperature of solidified wasteforms buried within deep strata landfills. Therefore, the thermal stability of the wasteform becomes very important. Further, the main strength-building phase in cement is the hydrated C-S-H (calcium-silicate-hydrate) phase, and radiolysis generates radiolytic hydrogen, which presents a hazard [65]. The problem related to radiolytic hydrogen can be solved by dehydrating the cement. However, dehydrating cement by heating treatment can severely impact the cement structure and mechanical properties since water is an essential component of the C-S-H phase [4]. Also, the $Ca(OH)_2$ phase decomposition in OPC occurs at ~500 °C and results in the disintegration of cement [63], which is undesirable, especially from a conditioning and safe storage point of view.

The freeze-thaw (F-T) behavior of OPC and its derivatives is problematic since it can lead to microscopic/macroscopic cracking from the expansion/contraction of hydrous phases [4]. Cement absorbs and retains moisture when exposed to repeated freeze-thaw cycles. As a result, the pore water in OPC expands during the freezing cycles and leads to internal micro/macro cracking, resulting in lower compressive strength [66]. For example, a study reported a decrement of ~10-15% in the compressive strength of OPC after 15 freeze-thaw test cycles (one cycle of 7 h: −20 °C for 3 h and 20 °C for 4 h) [58]. The freeze-thaw problem can be minimized by dehydrating cement but at the cost of degradation in the cement structure and properties. Relative to Cs-doped FA-

based AAM, F-T induced loss of compressive strength observed in Cs-doped OPC was almost 3.8 times higher after fifteen test cycles [58]. In a related study, Xu et al. [67] subjected Sr-loaded metakaolin-based AAM and OPC blocks to fifteen F-T cycles, and their results indicated about 9.4% reduction in compressive strength of the former and 21% for the latter. Pareek et al. [68] also investigated the F-T durability of normal strength concrete made of recycled aggregate and high-density OPC concrete (made with steel ball aggregates) to be utilized for the radiation-shielding of Cs-contaminated soil. Test results showed approximately 80% and 0% drops in the relative dynamic modulus of elasticity of the normal strength and high-density concrete mixtures after one-fifty F-T cycles, respectively. Therefore, over an extended period of exposure to F-T cycles, normal strength, OPC concrete mixtures made with recycled aggregates are unsuitable for radioactive shielding of radionuclides. Therefore, the freeze-thaw behavior of OPC-based systems is unfavorable for the immobilization of Cs and Sr.

In summary, the long-term durability of the OPC exposed to environmental weathering and the potential for the leaching of radionuclides through micro-cracks is a huge source of concern. This is particularly critical because many radionuclides with long half-life remain hazardous over a long period. The transport of groundwater through cracks would vitiate the cement matrix microstructure, causing the degradation of radionuclide-bearing cement phases and ion leaching. Due to the limitations mentioned above in the OPC systems for Cs and Sr immobilization, alternative low-cost and environmentally friendly materials that are thermally and chemically stable are required for the conditioning of wastes. Therefore, to reduce the leaching susceptibility of nuclear waste containment facilities, more durable alkali-activated alumino-silicate matrices (AAMs) have been proposed. The main attraction for alkali-activated matrices is the lack of

metastable hydrates, the precipitation of C-S-H with low Ca/Si ratio, and excellent resistance to deleterious solutions [69].

3. Immobilization of radionuclides in alkali-activated matrices

Alkali-activated materials (AAMs) such as geopolymers, also known as low-temperature inorganic cementitious aluminosilicate binders or alkali-bonded ceramic, have gained attention for effective immobilization of hazardous waste owing to their excellent environmental stability [69–71]. In addition, a wide array of characteristics such as tunable chemical composition, easy processing, good thermal and mechanical properties further endorse the suitability of AAMs as robust immobilization matrices for various hazardous elements such as Cs, Sr, Pb, Cd, Co, and Cr [70,72,73]. From the immobilization stance of hazardous cations, the amorphous or semi-crystalline three-dimensional network structure of geopolymers mainly consists of SiO_4 and AlO_4 tetrahedra linked alternately by sharing the oxygen atom [74,75]. The Al^{3+} in IV-fold coordination in the GP framework are charge-balanced by cations such as alkali metal or hazardous metal counterions [76]. This interaction facilitates physical immobilization through electrostatic attraction and impedes the leaching of cations through the geopolymer matrix. Further, upon heat treatment, the solidified waste form can be transformed into a stable crystalline phase of the hazardous element, resulting in chemical immobilization. The durable chemical bond can effectively restrict diffusion from the inner to the outer surface of the geopolymer matrix [77].

3.1 Immobilization of cesium in alkali-activated matrices

As discussed previously, the effective diffusion coefficients (D_e) of waste forms derived from Ordinary Portland cement typically fall within the range of 10^{-7} to 10^{-8} cm²/s for Cs immobilization, and their *LX* values are typically around 7.0. AAMs on the other hand have demonstrated a wide range of D_e and *LX* values for Cs immobilization, **Table 6**.

The room temperature cured AAMs such as Metakaolin-based geopolymer (GP), as discussed by He et al. [78], and the fly ash-based GP by Jain et al. [79] exhibited *LX* values ranging from 6.6 to 8.9. Notably, these values are comparable to or higher than those for traditional Ordinary Portland Cement (OPC)-based systems (**Table 6**). Haddad et al. [80] observed an enhancement in *LX* values (10–10.8) for metakaolin-GP systems when cured at 40 °C for 1 week, 1 month, and 3 months. Similarly, Jang et al. [49] reported *LX* values of 10–10.2 for fly ash-based GP systems cured at 60 °C for 24 hours, followed by additional curing at 20 °C for four weeks. In an effort to improve *LX*, He et al. [78] attempted to form pollucite in the metakaolin-based GP system through elevated heat treatment at 1000 °C for 2 hours, resulting in *LX* values ranging from 8.9 to 12.6, depending on the Na/Cs ratios in the mix design. The recent studies by Jain et al. [79,81,82] focused on fly ash-based GP systems cured at 90 °C for 7 days, demonstrating relatively high *LX* values within the range of 12.0–14.6. The improvement in Cs immobilization was attributed to the *in-situ* formation of pollucite in the fly ash-based GP matrix, leading to very low D_e values (~2.5×10^{-15} cm²/s), indicating negligible Cs leaching. This D_e value is approximately 8 orders of magnitude lower than that for the traditional OPC-based system (assuming $LX = 7$).

Table 7 provides a concise summary of all the experimental conditions and comparative analyses detailed in the following section.

Table 6
Summary of the effective diffusivities D_e and leachability indexes *LX* of different alkali-activated materials (AAMs) for cesium (Cs) immobilization.

Material	Test method	*De* (cm²/s)	*LX*	Reference
MK-GP		$1.7 \text{ to } 9\times10^{-11}$	* 10.0–10.8	Haddad et al. [80]
MK-GP (~22 °C curing)	ANSI/ANS 16.1	* 2.5×10^{-7} to 4×10^{-8}	6.6–7.4	He et al. [78]
MK-GP (1000 °C curing)		* 1.2×10^{-9} to 2×10^{-13}	8.9–12.6	
AABFS	ANSI/ANS 16.1	1.0×10^{-9} to 1.6×10^{-8}	7.0–7.8	Komljenović et al. [83]
FA-GP (in DI water)		2.6×10^{-11} to 1.8×10^{-11}	10.6–10.7	Deng et al. [84]
FA-GP (in seawater)		2.0×10^{-9} to 6.3×10^{-10}	8.7–9.2	
FA-GP		$1.2 \text{ to } 1.8\times10^{-10}$	10.0–10.2	Jang et al. [49]
FA-GP	ANSI/ANS 16.1	NA	NA	Li et al. [58]
FA-GP		NA	NA	Fernandez-Jimenez et al. [85]
FA-GP (22 °C curing)		5×10^{-8} to 1×10^{-10}	7.3–10.0	Jain et al. [79,81,82]
FA-GP (90 °C curing)		1×10^{-12} to 2.5×10^{-15}	12.0-14.6	

* Estimated values calculated from D_e or *LX* values, whichever was available in the literature. NA – Not available. Where MK-GP: Metakaolin-based geopolymer; AABFS: Alkali-activated blast furnace slag; FA-GP: Fly ash-based geopolymers.

Table 7
Comparative summary of experimental conditions and key findings for cesium immobilization in alkali-activated materials (AAMs).

Study	Synthesis method	Curing conditions	Cesium dosage	Leaching protocols/media	Key findings
Fernandez-Jimenez et al. [85]	Class-F FA + 8M NaOH (sol^n/solid = 0.4)	85 °C or 120 °C for 5h and 7d	1 wt.% (CsOH or $CsNO_3$)	TCLP (acetic acid in deionized water) & ANS 16.1 (Deionized water)	Cs associated with geopolymer gel; no distinct hydrated Cs compounds found; incorporating a low Cs dosage did not negatively impact the mechanical strength or microstructure of FA-GP.
Li et al. [58]	Class-F FA + NaOH + Na_2SiO_3 (SiO_2/Na_2O = 1.5)	60 °C for 27 days	2 wt.% ($CsNO_3$)	Deionized water, sulfuric acid, magnesium sulfate	GP showed superior immobilization compared to OPC in deionized water at 25 °C and 70 °C; *CFL* of GP in the magnesium sulfate solution was reported to be only 5% compared to OPC.
Deng et al. [84]	Class-F FA + NaOH + Na_2SiO_3 (SiO_2/Na_2O = 1.4)	40 °C for 28 days	2 wt.% ($CsNO_3$)	ANSI/ANS-16.1 Deionized water, groundwater, seawater	Irradiated FA-GP showed slight increase in *CLF* (5% more in deionized water) than non- irradiated FA-GP; irradiation effect was more noticeable in a seawater medium; *LX* values exceeded the minimum required value of 6.0 in all cases.
Jang et al. [49]	Class-F FA + 9M NaOH + Na_2SiO_3 (1:1 ratio) (soln/solid = 0.5)	60 °C for 24h, then 20 °C for 4 weeks	1 wt.% (CsCl)	ANSI/ANS-16.1 Deionized water	FA-GP showed superior physical encapsulation with smaller critical pore diameter (50-151 nm) compared to PC (284 nm); *LX* values for Cs: 10-10.2 for FA-GP, 7.0-8.0 for OPC and slag-blended geopolymers.
Kuenzel et al. [86]	MK + sodium or potassium-based activator	Ambient temperature (22 ± 3 °C) for 14 days	CsOH	European Standard BS EN 12457-2:2002 Deionized water	Sodium-based activators exhibited lower leaching of Cs^+ ions compared to potassium-based activators; Cs^+ preferentially binds to aluminate phases.
Komljenović et al. [83]	BFS + Na_2SiO_3 (SiO_2/Na_2O = 1.9)	95 °C for 1 day, then at RT till test	CsCl (2 and 5 wt.% Cs)	ANSI/ANS-16.1 Deionized water	A two-stage leaching process with an initial rapid leaching phase followed by slower diffusion-controlled leaching was observed; *LX* values ranged from 7.0 to 7.8. Cs incorporation positively impacted strength development, although some strength loss (4.5% to 22.6%) was noted after leaching.

Study	Synthesis method	Curing conditions	Cesium dosage	Leaching protocols/media	Key findings
Jain et al. [79,81,82]	Class-F FA + 5 to 11M NaOH (NaOH sol^n/FA = 0.4)	22 °C - 90 °C for 7 to 28 days	$CsOH.H_2O$ (2-20 wt.% of Cs)	ANSI/ANS-16.1 Deionized water	Enhanced Cs immobilization was achieved with *in-situ* pollucite crystallization with very low D_e value (2.5×10^{-15} cm^2/s); higher Cs dosage led to higher *LX* values (11.5-14.5); improved Cs immobilization with extended curing time; diffusion was found to be the primary leaching mechanism; JMAK model established for pollucite crystallization kinetics, indicating effective Cs immobilization at relatively low temperatures.

Where FA: Fly ash; MK: Metakaolin, BFS: Blast furnace slag, sol^n = solution, RT = Room temperature, Cs = Cesium.

Initial investigations into fly ash-based geopolymers (FA-GP), or alkaline-activated fly ash (AAFA), for cesium (Cs) immobilization were conducted by Fernandez-Jimenez et al. [85]. AAFA was synthesized by activating class-F fly ash with an 8 M NaOH solution at a solution/fly ash ratio of 0.4. The Cs dosage, constituting 1 wt.% of the initial fly ash content, was introduced either as CsOH or $CsNO_3$ dissolved in the alkaline activator. AAFA specimens were subjected to curing in an oven for 5 hours and 7 days at temperatures of 85 °C or 120 °C. Leaching studies employed the Toxic Characteristic Leaching Procedure (TCLP) and American Nuclear Society (ANS) 16.1 leaching protocols. The primary objectives of the investigation were to evaluate the influence of cesium salts (CsOH and $CsNO_3$) on the mechanical properties and mineralogical composition of AAFA and to examine the impact of curing time and temperature on Cs leaching behavior. Results indicated a chemical association of Cs with the amorphous geopolymer gel, suggesting the absence of distinct hydrated Cs compounds; however, quantitative validation was not provided. Although Cs-bearing zeolite presence was not reported, zeolitic phases such as hydroxysodalite ($Na_4Al_3Si_3O_{12}OH$), herschelite ($NaAlSi_2O_6.3H_2O$) were observed in FA-GP systems cured at high temperatures (40−120 °C), albeit without Cs incorporation. Additionally, the study proposed that

incorporating a low Cs dosage (1–2 wt.%) did not adversely affect the mechanical strength or microstructure of FA-GP. Leaching results consistently indicated Cs concentrations in the leachate (following the ANS 16.1 leaching protocol) below the analytical detection limit of 1 ppm. Consequently, the study did not provide a detailed Cs leaching profile or leachability index. It was recommended to investigate FA-GP with higher Cs concentrations to enhance the understanding of the immobilization mechanisms.

Subsequently, Li et al. [58] carried out an extensive comparative investigation contrasting FA-GP with OPC systems for the immobilization of a simulated radionuclide, specifically $133Cs^{+}$. In this study, FA-GP was formulated by activating class-F fly ash with a solution of (NaOH and Na_2SiO_3), adjusted to a molar mass ratio of SiO_2/Na_2O = 1.5. The simulated radionuclide, introduced as $CsNO_3$ at a dosage of 2 wt.%, was incorporated into the activating solution. FA-GP specimens underwent curing at 60 °C for a duration of 27 days. Leaching tests for both FA-GP and OPC systems were conducted in solutions of deionized water, sulfuric acid, and magnesium sulfate. Additionally, the thermal stability of these matrices was assessed in terms of high-temperature and freeze-thaw resistance. The leaching results of FA-GP and OPC in deionized water at temperatures of 25 °C and 70 °C exhibited superior immobilization of $133Cs^{+}$ in the FA-GP matrix, irrespective of temperature, as illustrated in **Figure 7**.

The cumulative fraction leached (*CFL,* cm) of cesium in the study was expressed by **Eq. 3**:

$$\boldsymbol{CFL = \left(\frac{\sum a_n}{A_0}\right)\left(\frac{V}{S}\right)} \qquad \textbf{Eq. 3}$$

where a_n = weight of radioactive element in leaching cycle n (g), A_0 = initial weight of radioactive element (g), S = contact area with the leachant (cm^2), V= volume of specimen (cm^3).

The cumulative fraction leached (*CFL*) of Cs from FA-GP was reported to be merely 5.4% of that

observed in OPC at 25 °C and 6.1% at 70 °C. Similarly, the *CFL* of FA-GP in the magnesium sulfate solution was reported to be only 5% compared to OPC. However, leachability index values were not reported in the context of these leaching studies. Nevertheless, it was suggested that the incorporation of Cs had an insignificant impact on the microstructure and mineral phases of FA-GP. Additionally, it was also postulated that Cs might be associated with geopolymerization products, although direct evidence to support this conjecture was not provided.

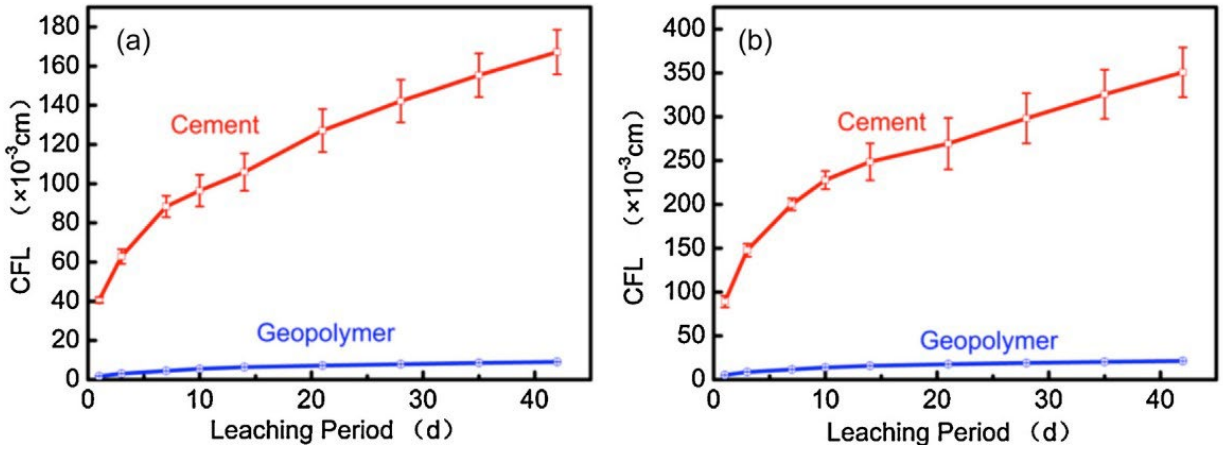

Figure 7: Leaching study by Li et al. [58] showing cumulative fraction leached (*CFL*) of cesium with leaching period in deionized water: (a) 25 °C, (b) 70 °C.

Deng et al. [84] examined the impact of gamma-ray irradiation, sourced externally from ^{60}Co, on the leaching behavior of simulated $^{133}Cs^{+}$ radionuclides from FA-GP wasteforms. FA-GP was produced by activating class-F fly ash using an alkali solution comprising sodium silicate and sodium hydroxide, with a molar mass ratio of $SiO_2/Na_2O = 1.4$. The simulated radionuclide 133Cs (2 wt.% Cs dosage) was introduced in the form of $CsNO_3$. The curing process for FA-GP wasteforms involved maintaining them at 40 °C for 28 days. Leaching tests were executed by immersing the wasteforms in deionized water, ground water, and seawater in accordance with the ANSI/ANS 16.1 method. The outcomes indicated that gamma rays did not induce notable morphological alterations in FA-GP, such as deformation, damage, or cracking, except for changes

in the distribution of pore sizes. Moreover, the cumulative leaching fraction (*CLF*) of Cs from irradiated FA-GP increased by only 5% compared to non-irradiated FA-GP in deionized water, as depicted in **Figure 8**. The leachability index (*LX*) values for irradiated and non-irradiated FA-GP in deionized water were reported as 10.7 and 10.6, respectively, suggesting an insignificant impact of irradiation on Cs leachability. Nevertheless, the irradiation effect was more noticeable in a seawater medium, where *LX* values of 8.7 and 9.2 were reported for irradiated and non-irradiated FA-GP, respectively. In summary, the results demonstrated that FA-GP could effectively immobilize Cs, even when submerged in seawater. Additionally, all reported *LX* values exceeded the minimum required value of 6.0 according to regulations. The study recommended further exploration into the effects of gamma-ray irradiation on damage mechanisms that could potentially occur in FA-GP systems.

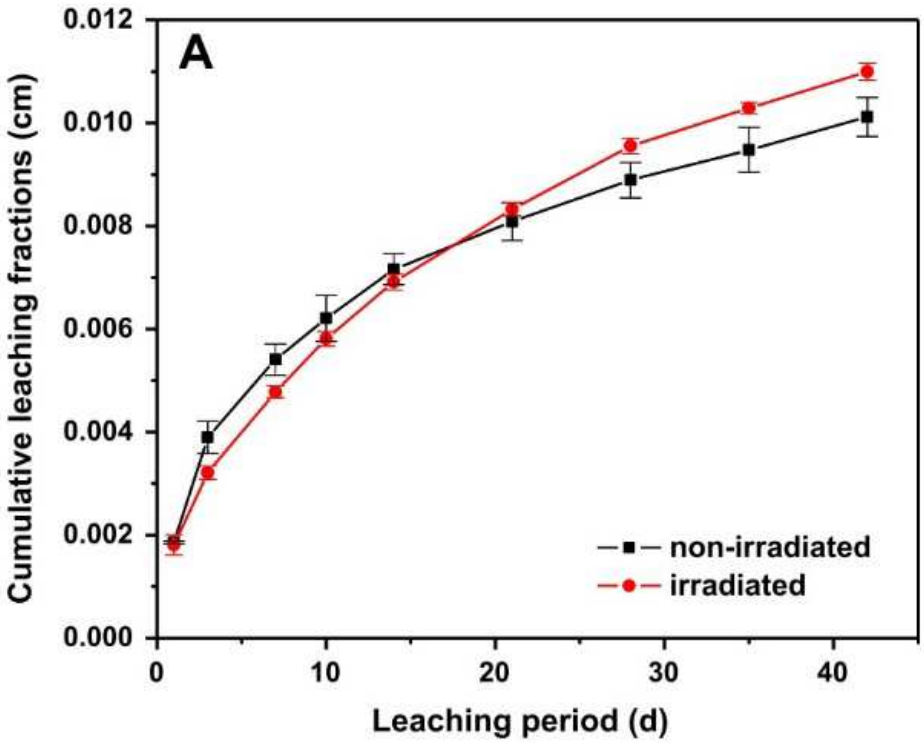

Figure 8: Cumulative leaching fractions (*CLF*) of cesium from geopolymer wasteforms in deionized water reported by Deng et al. [84].

The investigation conducted by Jang et al. [49] focused on the physical immobilization of Cs radionuclides in FA-GP, slag-blended geopolymers, and OPC systems. The synthesis of FA-GP involved activating class-F fly ash with an activating solution, maintaining a solution-to-solid ratio of 0.5. The alkali activator, with a weight ratio of 1:1, comprised a mixture of a 9M NaOH solution and a sodium silicate solution (SiO_2 = 29 wt.%, Na_2O = 10 wt.%, H_2O = 61 wt.%, specific gravity = 1.38). Stable isotopes of CsCl were utilized to mimic radioactive isotopes, and the Cs^+ incorporation into the matrix was set at 10 g/L (10,000 ppm or 1 wt.% of fly ash content) relative to the volume of all wasteform simulants. The initial setting of FA-GP occurred at 60 °C for 24 hours, followed by curing at 20 °C for four weeks before demolding. Leaching behavior assessment of cesium from these systems was conducted according to ANSI/ANS-16.1 standards. Reported *LX* values for cesium ranged between 10-10.2 for the FA-GP systems, whereas for OPC and slag-blended geopolymers, they ranged between 7.0-8.0. The relationship between critical pore diameter and the effective diffusion coefficient (D_e) of water-soluble Cs^+ ions was established (**Figure 9**). Critical pore diameter, defined as the diameter with the largest fraction of interconnected pores influencing transport properties, served to describe the connectivity of the cementitious material. FA-GP exhibited a critical pore diameter ranging from 50-151 nm, notably smaller than that of PC (284 nm). Consequently, FA-GP demonstrated superior physical encapsulation ability, effectively retarding the diffusion of Cs nuclides, in comparison to OPC or slag-based systems.

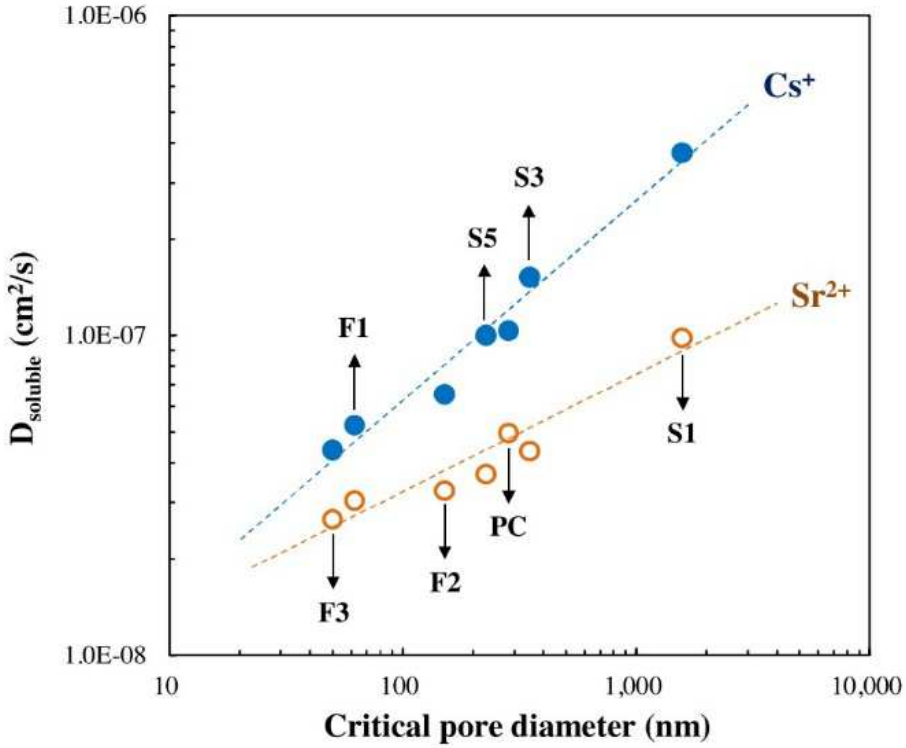

Figure 9: Relationship between the critical pore diameter of the binder and the diffusivity of water-soluble ions such as cesium (Cs) and strontium (Sr) reported by Jang et al. [49]. In the figure, F, S, and PC stand for fly ash-based geopolymers, slag-based geopolymers, and ordinary Portland cement, respectively.

The study by Kuenzel et al. [86] suggested that the specific activator employed in the activation of alkali-activated cement (AAC) could also have a significant influence on the immobilization efficiency of Cs^+ ions. The research indicated that AACs activated with sodium-based activators exhibited a lower leaching of Cs^+ ions in comparison to those activated with potassium-based activators. The Cs^+ ions, characterized as weak Lewis acids, tend to preferentially bind to aluminate phases during the formation of the AAC matrix, displacing sodium ions in the gel structure, as aluminate acts as a weak Lewis base.

In the study conducted by Komljenović et al. [83], the mechanical and structural properties of alkali-activated binders (AAB) based on blast furnace slag (BFS) doped with 2 and 5 wt.% Cs were investigated. The study identified a two-stage leaching process, with an initial rapid leaching

of non-bound or loosely bound ions followed by slower diffusion-controlled leaching. The addition of cesium to AABFS positively impacted its strength development, but some strength loss (between 4.5% to 22.6 %) was observed after leaching. Cesium was found to be preferentially associated with alkali-aluminosilicate gel, and correlations were established between compositional ratios and compressive strength. Additionally, aluminum released during leaching remained within the AABFS matrix, triggering gel reconstruction processes. The *LX* values were reported between 7.0 and 7.8 for the AABFS cured at 95 °C for 1 day.

The recent research conducted by Jain et al. [79,81,82] aimed at developing low-temperature effective and sustainable techniques for immobilizing cesium (Cs) in nuclear waste using NaOH-activated fly ash-based geopolymers (FA-GP). In the initial investigation [79], the authors identified key factors that affected Cs immobilization, such as curing temperature and the interaction between Cs dosage and curing temperature, **Figure 10**. FA-GP cured at 90 °C demonstrated superior Cs immobilization performance, notably with *in-situ* pollucite crystallization. It was reported that the combination of the chemical (within the amorphous gel and zeolitic phase) and physical (adsorbed on surfaces and trapped within porosity) immobilization of Cs in FA-GP resulted in the very low D_e value of 2.5×10^{-15} cm^2/s, which is ~ 8 orders of magnitude lower than the traditional OPC-based system.

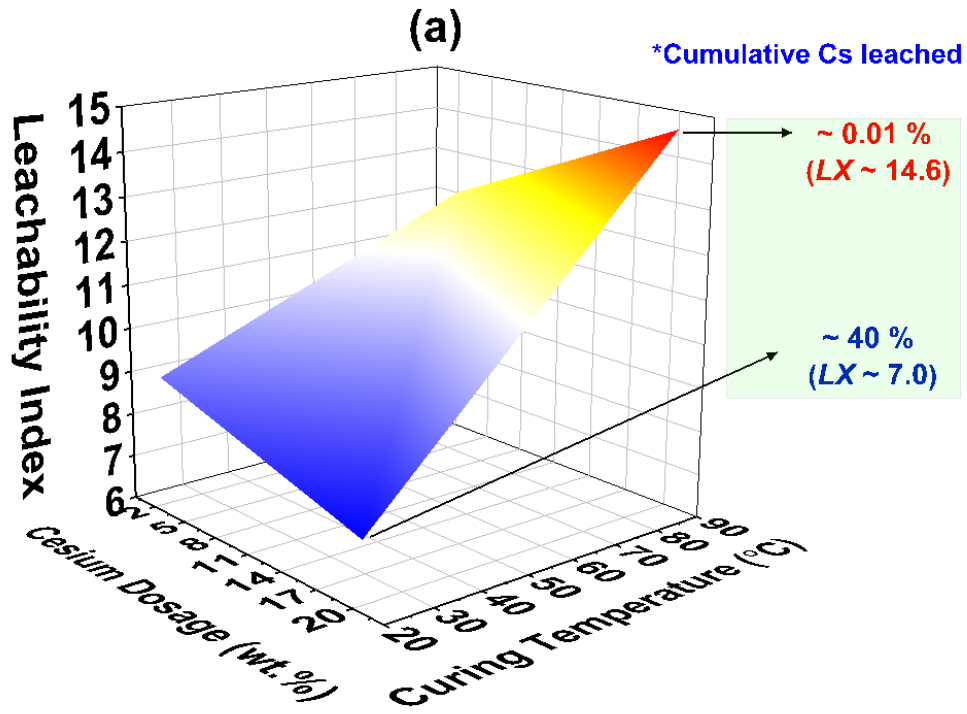

* Cumulative cesium leached (%) from FA-GP containing 20 wt.% Cs after five days leaching period

Figure 10: Effect of cesium dosage and curing temperature on the *LX* of 5M NaOH-activated FA-GP after (a) 7 days [79].

Subsequently, the authors examined Cs dosage and curing time effects on Cs leaching behavior (kinetics and mechanisms) and immobilization in FA-GP [81], emphasizing the significant role of *in-situ* pollucite formation. The results suggested that Cs dosage affected the resulting phase compositions and pore structure of FA-GP, eventually influencing the Cs immobilization in these matrices. The leaching behavior depended on the Cs dosage, **Figure 11**. It was suggested that the higher dosage (≥ 8 wt.%) of Cs provided conditions for *in-situ* pollucite crystallization within the FA-GP matrix and resulted in a significant increase in the *LX* values, e.g., from 11.5 (for 5 wt.% Cs) to 14.5 (for 20 wt.% Cs). Further, it was revealed that the cumulative leached fraction and the leaching rate of the room-temperature cured FA-GP improved significantly with an extended curing time of 180 days, irrespective of the Cs dosage. Furthermore, diffusion was suggested to be

the primary mechanism governing the leaching of Cs in the FA-GP systems.

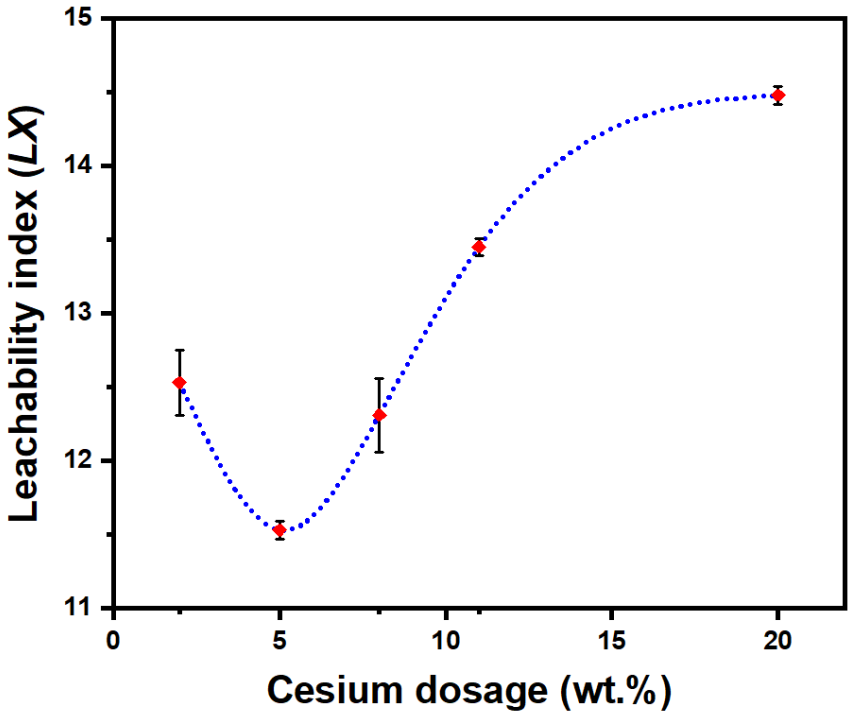

Figure 11: Effect of cesium dosage on the immobilization performance (*LX*) of fly ash-based geopolymers (FA-GP) cured at 90 °C for 7 days [81].

Finally, the authors explored the kinetics of *in-situ* pollucite crystallization in FA-GP systems (containing 20 wt.% Cs) using the JMAK model and determined a linear correlation between pollucite content, Cs immobilization, and various FA-GP properties [82]. It was suggested that the Cs immobilization (*LX*) improved as the amount of *in-situ* pollucite content in the FA-GP systems (containing 20 wt.% Cs) increased with curing time, **Figure 12**. Further, it was shown that the amorphous phase in the FA-GP systems transformed primarily into the crystalline phase of pollucite. The JMAK kinetics model for *in-situ* pollucite crystallization in the FA-GP system was established, and sigmoid types of curves were obtained, **Figure 13**. A low activation energy (~25 kJ/mol) indicated feasible pollucite crystallization and effective Cs immobilization at relatively low temperatures.

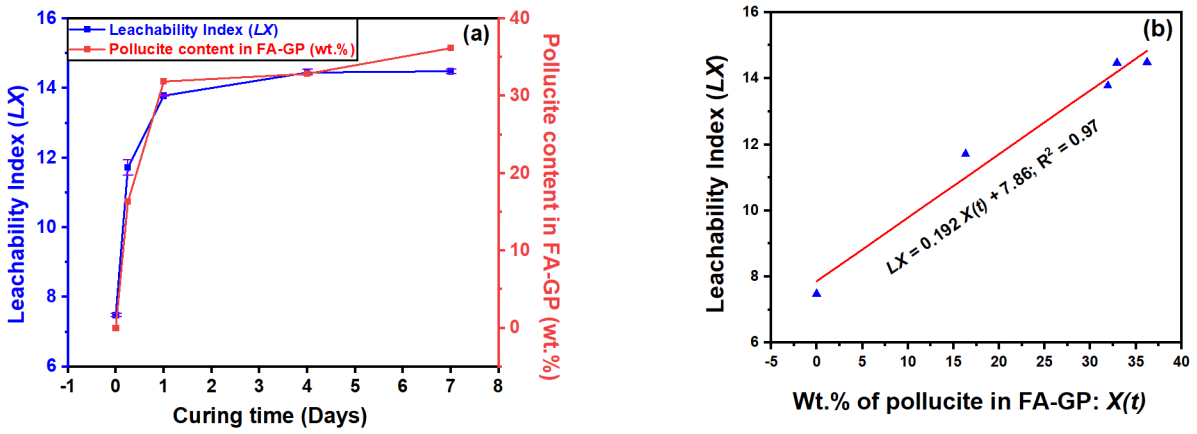

Figure 12: (a) Leachability index (left vertical axis) and pollucite content (wt.% within ±0.4 SD) in FA-GP (right vertical axis) as a function of curing time and (b) Linear relationship between leachability index (LX) and wt.% of pollucite formed X(t) in 90 °C cured FA-GP systems containing 20 wt.% Cs dosage [82].

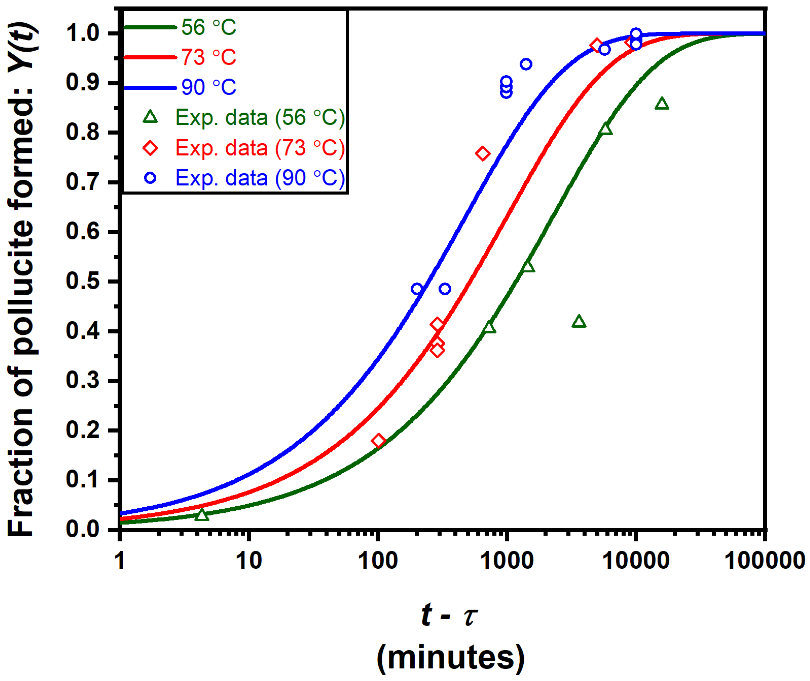

Figure 13: JMAK kinetic model for pollucite crystallization in the FA-GP systems (containing 20 wt.% Cs) for three different temperatures (56, 73, and 90 °C) along with the experimental data [82].

Collectively, these findings have shown AAMs as a promising material for efficient and sustainable Cs immobilization in nuclear waste, demonstrating the potential for controlled Cs immobilization and long-term storage applications.

3.2 Immobilization of strontium in alkali-activated matrices

In OPC matrices, the presence of a high amount of bound water and the occurrence of Sr^{2+} adsorption on partly hydrated cement phases via reversible ion-exchanges creates potential environmental release risks [87]. Therefore, matrices such as AAMs that attain full hydration with less water within a short period of time are more favorable for Sr^{2+} immobilization. Furthermore, the high ion-exchange capacity and the similarity in the dense network of SiO_4 and AlO_4 tetrahedrons makes the AAM a formidable zeolite precursor [88] with a huge number of exchange sites where alkali ions could be substituted with radionuclides. The most common aluminosilicate precursor materials used in synthesizing AAMs for Sr^{2+} immobilization are metakaolin, coal fly ash, and ground granulated blast furnace slag (GGBS). **Table 8** illustrates the effective diffusivity (D_e) range concerning the immobilization of Sr in different Alkali-Activated Materials (AAMs), encompassing fly ash/slag-based and metakaolin-based geopolymers. The D_e values documented in AAMs are either comparable or lower than those observed in conventional Ordinary Portland Cement (OPC)-based systems for Sr immobilization, indicating their viability as robust candidates for the immobilization of Sr.

Table 8
Summary of the effective diffusivities D_e of different alkali-activated materials (AAMs) for Strontium (Sr) immobilization.

Material	Test method	Effective diffusion coefficient D_e (cm^2/s)	Reference
FA – AAM (L/S = 0.5)	ANS 16.1	6.8×10^{-15} to 1.3×10^{-14}	Jang et al. [49]
FA + slag – AAM (L/S = 0.5)		2.1×10^{-13} to 5.1×10^{-12}	
MK-GP (Room temperature)	ANS 16.1	3.2×10^{-10}	Jia et al. [89]
MK-GP (600 °C)		5.0×10^{-11}	
MK-GP (800 °C)		1.0×10^{-8}	
MK-GP (1000 °C)		3.2×10^{-9}	
MK-GP (1200 °C)		2.0×10^{-12}	

Where FA: Fly ash; MK-GP: Metakaolin-based geopolymer; AAM: Alkali-activated materials

Metakaolin, a very reactive and aluminum-bearing anhydrous form of the clay mineral kaolinite has been successfully used for the encapsulation of radionuclides. The retention efficiency increased as the Si/Al and Ca/(Si+Al) ratio in amorphous geopolymer gels decreased. Results from the study by Walkley et al. [90] showed that Sr^{2+} are easily accommodated in amorphous (N,K)-A-S-H in metakaolin-based AAM cured at 20°C by displacing some of the alkali cations from the extra-framework sites and decreasing the Si/Al ratio of the gel. Sr^{2+} also promoted the formation of zeolite A (Linde Type A-LTA) and Sr-partially substituted zeolite Na-A in samples cured at 80°C. With the micro pores in these zeolites, Sr could be easily exchanged with cations loosely bound to the framework structure. Xu et al. [91] was of the opinion that Sr^{2+} is typically incorporated in zeolite framework structure, acting as the charge balancing cation.

Relative to OPC matrix, Jang et al. [49] showed that reduced critical pore diameter and capillary pore volume in fly ash-based AAM was instrumental to the decreased diffusivity of Sr^{2+} they

observed. Liu et al. [92] showed that the lower total porosity of fly ash-slag-metakaolin–based AAM compared to OPC is responsible for the reduced leaching of Sr^{2+} observed in the former. Tian and Sasaki [93] investigated the stabilization of Sr^{2+} in fly ash-based AAM, and they reported that ion exchange with alkaline ions is the main process with free energy ranging from 9.56 to 14.56 kJ/mol, with no new phases formed afterward. Research findings by Jang et al. [49] also indicated that slag-blended AAM had higher capillary pore volume with widespread dispersion and elevated Sr^{2+} leaching relative to fly ash-based AAM. A related study by Vandevenne et al. [94] investigated the immobilization of Sr^{2+} in slag-based AAM, and their findings indicated that Sr^{2+} mainly precipitated as $Sr(OH)_2$, negatively affecting reaction kinetics of precursor materials, thereby stunting matrix strength development. Nonetheless, some research studies have shown that the drawback observed in slag-containing AAM could be ameliorated using binder material blending and hybridization. Relative to the plain slag-based AAM, Guangren et al. [95] reported reduced leaching of Sr^{2+} in slag-based AAM enriched with aluminum (metakaolin), and this development was ascribed to the production of (Na+Al)-substituted C-S-H and self-generated zeolite which had superior selective adsorption of Sr^{2+}. Huang et al. [96] reported that the addition of sodium hexametaphosphate slag-based AAM activated with sodium silicate/sodium hydroxide, and subsequently microwaved showed enhanced mechanical strength development and Sr^{2+} encapsulation.

Good resistance to elevated temperature-induced deterioration is another attribute that distinguishes AAMs from OPC, making the former more useful for radionuclide encapsulation. Relative to the Portland cement matrix, He et al. [97] showed that although increased storage temperature can enhance the release of the Sr^{2+}, its leaching rate in metakaolin AAM was still 100-200 times lower. Zeolite microspheres produced through *in-situ* thermal curing of slag-based AAM

blended with metakaolin were also shown to have enhanced adsorptive removal of Sr^{2+} from wastewater [98]. High temperature sintering (1100°C) of K-based metakaolin AAM-zeolite A composite has also been used to transform amorphous gel and zeolite A, creating a ceramic waste form that contains crystalline (leucite and Sr-feldspar) phases, that readily incorporate the Sr [99]. In general, the immobilization of radionuclides such as Sr^{2+} in AAMs can occur in three ways; physical adsorption, ion exchange, and hydrates encapsulation. Although the very high alkalinity of the AAM matrix ensures reduced solubility of the Sr^{2+}, the very dense microstructure and low porosity of these matrices are quite instrumental to the increased physical adsorption of radionuclides.

It has also been reported that the valence of radionuclides is also an important factor. The investigation by Xu et al. [91] showed that compared to monovalent cations, higher valence cations have a stronger affinity for the non-bridging oxygen sites in the silicate tetrahedron. Moreover, the ion exchange phenomenon whereby radionuclide cations with a comparable radius substitute charge-balancing alkali earth metal ions in negatively charged sites in hydrates structure is also another significant immobilization mechanism. The poorly crystallized C-S-H with broken bonds in AAMs allows easier substitution of Al^{3+} for Si^{4+}, thereby creating a net negatively charged aluminosilicate chains conducive for cation exchange. The open cavity/huge surface area of zeolite in the AAM is also favorable for the encapsulation of the Sr. Findings from these studies (Provis et al. [100]; Tian et al. [88]), the similarity in the dense network of SiO_4 and AlO_4 tetrahedrons makes the aluminosilicate hydrate gel ((N,K)-A-S-H), a formidable zeolite precursor or proto-zeolitic structure with a huge number of ion exchange sites. Blackford et al. [101] showed that Sr^{2+} can be partly and predominantly retained in amorphous (N,K)-A-S-H gel and crystalline $SrCO_3$, respectively. However, the encapsulation efficiency in AAM is also dependent on the size of these

ions; where with similarity in ionic radius and retention selectivity, the formation of zeolites is easier [102]. It has also been noted that the concentration of divalent cations such as Ca^{2+} and Mg^{2+} strongly influence Sr^{2+} exchange process, hence AAMs with low-calcium content and less dissolved Ca^{2+} in the pore solution are preferable [103]. Structural deformation that could affect pore size distribution in matrices after cation exchange is also another factor that influences the encapsulation of radionuclides. Indeed, Tian and Sasaki [93] reported that the substitution of monovalent cations with divalent cations with larger radius would lead to a reduction in pore space.

4. Durability requirements of cement and alkali-activated matrices

Fundamentally, cement-like materials such as Portland cement or AAMs are porous solids that consist of a complex blend of gel-like and crystalline phases, accompanied by an interstitial pore solution that maintains chemical equilibrium with the solid phase [69,104]. The proportion of various solid phases generated during hydration reactions is contingent upon factors such as the water-to-binder ratio, binder composition, and the inclusion of additives to aid in product placement and handling. If the purpose of the cementitious material is to immobilize or delay the release of hazardous wastes, the waste composition can also impact the final waste form's solid phase content. The physical characteristics of the matrix, including porosity, permeability, and conductivity, are influenced by both the composition of the solid phase and the quantity of coarse/fine aggregate typically incorporated to enhance strength and durability. Over time, a cementitious monolith may interact with different surrounding media, exposing it to water, dissolved constituents, or gases (including water vapor and air). The transfer of these substances between materials is influenced by the physical-chemical properties of the surrounding materials, which, in turn, are affected by the design of the engineered system. The surrounding media may comprise an open atmosphere (e.g., air in contact with above-ground vaults), steel (e.g., tank liners), soil or granular fill (compacted fill around buried structures, either unsaturated or water-saturated), or contained liquids (e.g., unlined spent fuel pools). In these scenarios, the cementitious monolith, serving as structural concrete, grout, or a waste form, may exhibit some degree of cracking, either initially or progressing over the monolith's lifespan. **Figure 14** provides a conceptual representation illustrating potential release processes, influential physical and chemical factors, and interfacial phenomena that may occur upon the introduction of a cementitious barrier into the environment [105].

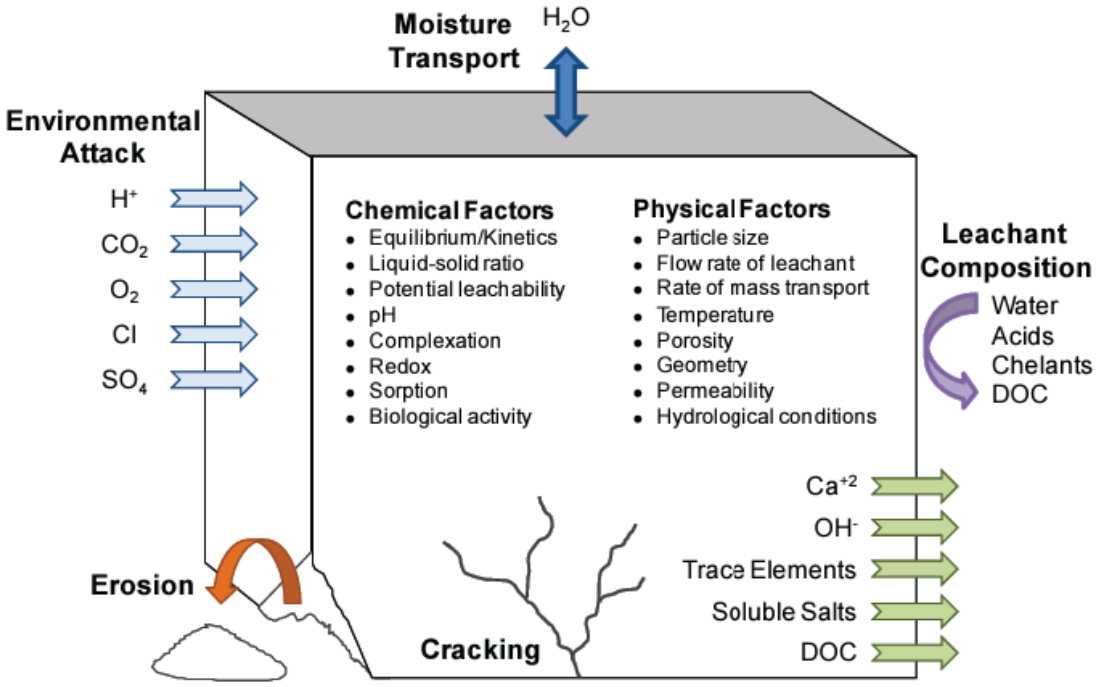

Figure 14: Internal factors and external phenomenon that can influence the leaching process in cementitious materials [105]. Here, DOC in the figure refers to the degree of carbonation.

Therefore, ensuring the robust durability of waste forms becomes crucial for the extended storage of nuclear waste, assuring the effectiveness of the engineered barrier system over the long term.

4.1 The effect of leaching temperature on cesium and strontium immobilization and leaching rates

Although the influence of temperature on the microstructure and phase composition of cement and AAMs is well-known, its effect on the leaching of radionuclides is not fully clarified. Fuhrmann et al. [106] showed that the leaching of radionuclides from solid cement waste forms not only accelerated with increasing temperature, the leaching of Sr was also transformed from diffusion-controlled to a different mechanism at temperatures above 50 °C. In addition, Cs was suggested to be leached by diffusion mechanism (regardless of the temperature) that is modified by adsorption possibly on calcium carbonate that formed on the surfaces of the waste forms [106]. Erdemoğlu

and Canbazoğlu [107] investigated the leaching of strontium sulfide (SrS) with water, and their findings indicated that precipitates such as $Sr(OH)_2$ became more soluble with increases in temperature, thereby making Sr more susceptible to leaching.

Papadokostaki and Savidou et al. [43] studied the leaching mechanisms of Cs ions incorporated in Ordinary Portland Cement at 30 °C and 70 °C. The long-term leaching experiments revealed an expedited elution process, a phenomenon not discernible in short-term leaching tests. This acceleration was linked to increased porosity arising from the erosion of the cement matrix, particularly pronounced at elevated temperatures (70 °C). It was suggested that high temperature leaching could be useful as an accelerated test, which can detect deviations caused by erosion on a shorter time scale.

Li et al. [58] conducted long-term leaching tests on Cs-containing waste in deionized water at 25 °C and 70 °C, revealing that higher temperatures increased the cumulative leached fraction for both OPC and AAM systems. The transition from 25 to 70 °C escalated leaching rates in both AAM and cement matrices, likely due to an expanded pore diameter facilitating simulated radionuclide diffusion. Despite temperature variations, AAM (fly ash-based geopolymer) consistently demonstrated effective immobilization of $133Cs^+$, attributed to its lower total porosity, resulting in reduced permeability and ion diffusivity. Compared to cement, alkali-activated fly ash-based geopolymer proved more suitable for Cs immobilization.

4.2 The effect of freeze-thaw cycles on cesium and strontium immobilization and leaching rates

Temperature cycling due to weather/seasonal changes can also lead to the development of residual strains and thermal cracking of solid monoliths. Xu et al. [108] investigated the thermal durability of Sr-loaded zeolite encapsulated in either cement or metakaolin-AAS solid, and they observed

that while cement blocks experienced significant micro cracking and loss of compressive strength on exposure to high temperatures and freeze-thaw temperature cycles, AAS blocks showed no micro-cracking and limited strength loss. Cyclic expansion/contraction of AAM waste forms subjected to freeze-thaw loading could lead to the gradual development of leaching-enhancing micro-cracks. A few studies (Li et al. [58]; Xu et al. [91]; Tan et al. [109]) showed that compared to OPC matrices, Cs and Sr-bearing AAMs had a superior structural resistance to freeze-thaw degradation, losing just 4-10% of the initial compressive strength after 15 freeze-thaw cycles. However, a related study by Li et al. [110] indicated that the freeze-thaw durability of Sr-bearing AAM was dependent on the number of cycles, the loss of compressive strength increasing to about 20% after 45 freeze-thaw cycles, albeit without compromising the immobilization of the Sr radionuclide. Therefore, given that the waste forms evaluated were subjected to a limited number of freeze-thaw cycles, long-term freeze-thaw studies investigating the solubility of radionuclides and its effect on the ice crystallization temperature/pressure, and the associated water-saturation proclivity on the freeze-thaw resistance of waste forms are required.

4.3 The effect of carbonation on cesium and strontium leaching rates

Carbonation is the process whereby atmospheric CO_2 reacts with cement and AAM hydrates reducing the pH, densifying the microstructure, and increasing shrinkage cracking (Dayal and Readson et al. [111]; Houst and Wittmann et al. [112]; Van Gerven et al. [113]). Hence, for the long-term performance of waste forms, carbonation is an important factor to consider. Whereas carbonation by virtue of its transformation of portlandite to carbonates has been reported to reduce porosity thereby positively influencing the compressive strength of cement-based materials and sediments, it vitiates the strength of AAMs (Chen et al. [114]; Pandey et al. [115]). Moreover, carbonation-induced reduction of matrix pH is also quite critical because this could potentially

increase the solubility/leaching of radionuclides. Thus, it is imperative that for every waste form, the net implication of the competing carbonation consequences is clearly understood.

Palacios et al. [116] investigated the impact of severe carbonation conditions on pastes made of Portland cement (OPC) and alkali-activated slag (AAS). It was reported that the carbonation mechanisms differed between the OPC and AAS systems. In Portland cement pastes, carbonate precipitation occurred due to the higher Ca content, which interacted with H_2CO_3 during carbonation in both portlandite and C–S–H gel. On the other hand, alkali-activated slag (AAS) pastes underwent direct carbonation in the C–S–H gel.

Park et al. [117] investigated the carbonation-induced weathering effect on the Cs retention capacity of Portland cement paste. The results revealed that with an increased degree of carbonation, the extent of calcium removal from the hydration products also increased. The C-S-H was converted into decalcified silica gel, and the AFt/AFm phases were transformed into alumina gel. As a result, these changes corresponded to a negatively charged surface of the carbonated cement hydrates and consequently significantly enhanced the Cs adsorption capacity. The previous studies by Walton et al. [118]; Shafique et al. [119] and Bar-Nes et al. [120] have shown that carbonation decreased the release of Sr from cement-based waste forms. In addition to the reduced leachability of Sr, Venhuis and Reardon et al. [121] also reported reduced release of Cs from carbonated cementitious wasteforms.

In the study conducted by Tanasijević et al. [122], the influence of an accelerated carbonation process on both the leaching resistance and strength of alkali-activated blast furnace slag (AABFS) incorporated with 2% and 5% cesium (representing solidified simulated radioactive waste) was examined. The combination of accelerated carbonation and extended curing demonstrated a

positive effect on the efficiency of cesium immobilization in AABFS, as evidenced by an increase in the leachability index values from 7.8 to 9.0 (2 wt.% Cs) and from 7.0 to 8.5 (5 wt.% Cs).

The above studies suggest that carbonation in the cementitious waste forms can decrease the release of Sr and Cs into the environment, indicating potential benefits for radioactive waste containment.

5. Future trends, conclusions and recommendations

5.1 Novel immobilization materials and techniques

Among the novel techniques, spark plasma sintering (SPS) of powders, incorporating pressure, high temperature, and diffusion bonding, is employed for producing highly dense ceramics to immobilize radionuclides. Yarusova et al. [123] applied the high-temperature SPS technique to create dense aluminosilicate ceramic matrices with high sorption capacity and minimal Cs leaching propensity. In a related study, Shichalin et al. [124] also utilized the SPS technique to synthesize dense and strong $SrTiO_3$ ceramics with a perovskite structure. Characterization studies revealed negligible Sr leaching from $SrTiO_3$ ceramic monoliths [124]. Key features of the SPS technique include the potential for mixed ion-covalent bonding and the rapidity of the synthesis process.

It is widely accepted that the chemical immobilization of hazardous elements is more reliable than their physical immobilization [125]. In contrast to conventional curing of Alkali-Activated Materials (AAMs) at temperatures of 60-80 °C, high-temperature synthesis of AAMs has proven effective in forming crystalline phases such as leucite, pollucite, and analcime. Tian et al. [126] recommended geopolymers with SiO_2:$Al2O_3 \leq 2$ (molar ratios) to achieve a higher content of crystalline phases and improved Cs^+ immobilization effects. Various studies on metakaolin-based geopolymers (MK-GP) have aimed to chemically immobilize Cs by forming Cs-bearing zeolitic phases. For instance, heat treatment of Cs-containing amorphous metakaolin-based geopolymers at 900–1400 °C produced pollucite ($CsAlSi_2O_6$) or mixtures of pollucite and a feldspathoid phase $CsAlSiO_4$ [127,128]. However, these studies on pollucite crystallization in MK-GP systems involved complex steps like sintering at 1000–1200 °C, hot pressing (~750 °C), or hydrothermal treatments (>200 °C) [77]. Fu et al. (2020) [77] employed low-temperature (230 °C) hydrothermal synthesis of metakaolin-based AAM to produce Cs-immobilizing analcime and pollucite

crystalline phases. In a related study, Li et al. [129] demonstrated that high-temperature sintering at 1100 °C transformed metakaolin-based AAM-zeolite A to leucite, a crystalline phase highly favorable for immobilizing Cs and Sr.

In regards to low temperature crystallization of radionuclides, Jain et al. [11,79,81,82] conducted studies demonstrating that curing fly ash-based geopolymers (FA-GP) at temperatures <90 °C led to pollucite formation with low activation energy (25kJ/mol), resulting in a stable Cs-based crystalline phase of the radionuclide with high immobilization efficacy. Recently, Haddad et al. [80] investigated a relatively low-temperature curing regime at 40 °C for 3 months in MK-GP (with 50 wt.% of Cs dose) and reported the formation of Cs-bearing zeolite F-type. However, Cs-containing zeolitic phases were not detected for low Cs dosage (1 wt.%). Further, Wagh et al. [130] investigated ceramicrete, a chemically bonded phosphate ceramic with a struvite-K mineral structure synthesized under ambient conditions for immobilizing radioactive Cs. The findings revealed that Cs^+ effectively partially replaced K^+ in the K-struvite structure, resulting in the formation of (K, Cs)-struvite crystals. These crystals exhibited remarkably low leaching of Cs^+, even under elevated temperatures.

Radionuclide immobilization is a complex function of the composition and microstructure of the conditioning matrix. Therefore, to address the intricate challenge of immobilizing radionuclides effectively (especially Cs and Sr), it is essential to explore sophisticated, cost-effective techniques that prioritize matrix durability. Long-term leaching studies are crucial for evaluating sustained efficacy, and guiding the optimization of methods such as Spark Plasma Sintering (SPS) or low-temperature curing. Further, interdisciplinary collaboration among material scientists, environmental engineers, civil engineers, and nuclear researchers is key to developing environmentally responsible approaches for secure radionuclide immobilization.

5.2 Conclusions and recommendations

This review article explored various cementitious materials for the immobilization of cesium (Cs) and strontium (Sr) radionuclides, shedding light on the limitations of traditional Ordinary Portland Cement (OPC) matrices and the promising alternative materials. While OPC-based systems have demonstrated limitations in effectively immobilization of Cs and Sr due to their high solubility and diffusivity, unconventional materials like Sulphoaluminate cement (SAC) and Magnesium Potassium Phosphate (MPP) cement showed encouraging results for effective radionuclide immobilization. Moreover, Alkali-activated matrices (AAMs) have demonstrated significant potential in immobilizing Cs and Sr through electrostatic attraction and chemical bonding. Furthermore, the review article emphasized on the importance of various ageing processes and durability concerns, such as leaching temperature, freeze-thaw behavior and carbonation, which affects the microstructure of cement matrices and leaching rates of radionuclides. The need for comprehensive durability studies for long-term waste storage was discussed. In addition, discussions on innovative techniques such as spark plasma sintering (SPS) and low-temperature crystallization for enhancing radionuclide immobilization efficiency were incorporated in this article. A holistic integration of detailed research studies on these aforementioned ageing processes and emerging technologies will help in the development of an all-encompassing, sustainable nuclear waste management program.

It is recommended to investigate the effects of other ions present in low/intermediate-level nuclear waste (LILW) on the leaching behavior of cesium (Cs) and strontium (Sr) within OPC and AAM matrices. Simulating site-specific nuclear waste conditions would provide valuable insights into potential interference with radionuclide immobilization and crystalline phase formation.

It is further recommended to extend beyond the current short-term testing standard (ANSI/ANS 16.1) for radionuclide release from solidified LILW waste forms. Long-term leaching tests (>1 year) or accelerated tests under actual site conditions are recommended to better assess the performance of multi-barrier systems, such as concrete vaults, in long-term waste containment. Recognizing the potential changes in leaching rates and retention capacity of cementitious wasteforms over time, especially due to degradation processes and environmental factors, is deemed essential.

Additionally, it is recommended to investigate the effects of high concentrations of radioactive Cs or Sr on various properties of cementitious matrices, including phase composition, microstructure, compressive strength, pore size distribution, and durability. Exploring the potential for immobilizing other hazardous cations or heavy metals in AAM systems, such as Th, Pb, Cd, Co, and Cr, is advised based on promising results observed for Cs and Sr immobilization.

Durability considerations remain a focal point in the recommendations, with a suggestion for leaching studies under harsh conditions, including acidic, seawater, or sulfate-rich environments. These studies aim to evaluate the long-term stability of cementitious matrices in waste containment. Furthermore, it is recommended to investigate the impact of freeze-thaw cycles on these matrices, covering aspects such as microstructure, phase compositions, and immobilization behavior, to address potential deterioration issues, particularly in cold climates.

In summary, the above recommendations collectively aim to enhance the effectiveness, reliability, and understanding of cementitious matrices in the intricate task of immobilizing radioactive waste, contributing to the long-term safety and durability of waste containment systems.

Acknowledgments

The authors gratefully acknowledge financial support from the University of British Columbia, SERB-UBC Overseas Fellowship, Natural Sciences and Engineering Research Council of Canada Grants, and Canada-India Research Center of Excellence IC-IMPACTS.

6. References

[1] N. Tanaka, Energy Technology Perspectives 2008–scenarios and strategies to 2050, Int. Energy Agency (IEA), Paris 10 (2008).

[2] D.S. Siqueira, J. de Almeida Meystre, M.Q. Hilário, D.H.D. Rocha, G.J. Menon, R.J. da Silva, Current perspectives on nuclear energy as a global climate change mitigation option, Mitig. Adapt. Strateg. Glob. Chang. 24 (2019) 749–777. https://doi.org/10.1007/s11027-018-9829-5.

[3] M. Schneider, A. Froggatt, The World Nuclear Industry Status Report 2019, in: World Sci. Encycl. Clim. Chang., 2021: pp. 203–209. https://doi.org/10.1142/9789811213953_0021.

[4] E.R. Vance, D.S. Perera, Geopolymers for nuclear waste immobilisation, Geopolymers (2009) 401–420. https://doi.org/10.1533/9781845696382.3.401.

[5] IAEA, Climate change and nuclear 2015, J. Chem. Inf. Model. 53 (2015) 160. https://doi.org/10.1017/CBO9781107415324.004.

[6] IAEA, Climate Change and Nuclear Power 2015, Clim. Chang. Nucl. Power 2015 (2015) 1–112. https://www.iaea.org/publications/10928/climate-change-and-nuclear-power-2015 (accessed May 17, 2023).

[7] R.O.A. Rahman, R.Z. Rakhimov, N.R. Rakhimova, M.I. Ojovan, Cementitious Materials for Nuclear Waste Immobilization, John Wiley & Sons Ltd, 2014. https://doi.org/10.1002/9781118511992.

[8] IAEA, IAEA Safety Standards: Classification of Radioactive Waste - No. GSG-1, Gen. Saf. Guid. IAEA (2009) 68. https://doi.org/ISBN:978-92-0-109209-0.

[9] P.K. Andersen, A. Ghassemi, M. Ghassemi, Nuclear Waste, Encycl. Energy (2004) 449–463. https://doi.org/10.1016/B0-12-176480-X/00414-9.

[10] M.I. Ojovan, W.E. Lee, S.N. Kalmykov, Nuclear Decay, in: An Introd. to Nucl. Waste Immobil., Elsevier, 2019: pp. 9–22. https://doi.org/10.1016/b978-0-08-102702-8.00002-9.

[11] S. Jain, Fly ash-based geopolymers for immobilization of nuclear waste containing cesium, (2022). https://doi.org/https://dx.doi.org/10.14288/1.0422417.

[12] A.M. El-Kamash, M.R. El-Naggar, M.I. El-Dessouky, Immobilization of cesium and strontium radionuclides in zeolite-cement blends, J. Hazard. Mater. 136 (2006) 310–316. https://doi.org/10.1016/J.JHAZMAT.2005.12.020.

[13] M.I. Ojovan, W.E. Lee, S.N. Kalmykov, Nuclear Waste Processing Schemes, An Introd. to Nucl. Waste Immobil. (2019) 167–190. https://doi.org/10.1016/b978-0-08-102702-8.00013-3.

[14] D.L. Heiserman, Exploring chemical elements and their compounds, in: McGraw-Hill, 1992: pp. 201–203.

[15] M.P. Unterweger, D.D. Hoppes, F.J. Schima, New and revised half-life measurements results, Nucl. Inst. Methods Phys. Res. A 312 (1992) 349–352. https://doi.org/10.1016/0168-9002(92)90180-C.

[16] M.I. Ojovan, W.E. Lee, S.N. Kalmykov, Short-Lived Waste Radionuclides, in: An Introd. to Nucl. Waste Immobil., Elsevier, 2019: pp. 145–154. https://doi.org/10.1016/b978-0-08-102702-8.00011-x.

[17] J. Meija, T.B. Coplen, M. Berglund, W.A. Brand, P. De Bièvre, M. Gröning, N.E. Holden, J. Irrgeher, R.D. Loss, T. Walczyk, T. Prohaska, Isotopic compositions of the elements 2013 (IUPAC Technical Report),

Pure Appl. Chem. 88 (2016) 293–306. https://doi.org/10.1515/PAC-2015-0503.

[18] D.K. Gupta, U. Deb, C. Walther, S. Chatterjee, Strontium in the ecosystem: Transfer in plants via root system, Behav. Strontium Plants Environ. (2017) 1–18. https://doi.org/10.1007/978-3-319-66574-0_1.

[19] V. Höllriegl, H.Z. München, Strontium in the Environment and Possible Human Health Effects, Encycl. Environ. Heal. (2009) 268–275. https://doi.org/10.1016/B978-0-444-52272-6.00638-3.

[20] A. Burger, I. Lichtscheidl, Strontium in the environment: Review about reactions of plants towards stable and radioactive strontium isotopes, Sci. Total Environ. 653 (2019) 1458–1512. https://doi.org/10.1016/J.SCITOTENV.2018.10.312.

[21] V. Höllriegl, H.Z. München, Strontium in the Environment and Possible Human Health Effects, Encycl. Environ. Heal. (2011) 268–275. https://doi.org/10.1016/B978-0-444-52272-6.00638-3.

[22] S.K. Sahoo, N. Kavasi, A. Sorimachi, H. Arae, S. Tokonami, J.W. Mietelski, E. Lokas, S. Yoshida, Strontium-90 activity concentration in soil samples from the exclusion zone of the Fukushima daiichi nuclear power plant, Sci. Rep. 6 (2016). https://doi.org/10.1038/srep23925.

[23] W.J.F. Standring, D.H. Oughton, B. Salbu, Potential remobilization of 137Cs, 60Co, 99Tc, and 90Sr from contaminated Mayak sediments in river and estuary environments, Environ. Sci. Technol. 36 (2002) 2330–2337. https://doi.org/10.1021/ES0103187.

[24] J.T. Smith, S.M. Wright, M.A. Cross, L. Monte, A. V. Kudelsky, R. Saxén, S.M. Vakulovsky, D.N. Timms, Global Analysis of the Riverine Transport of 90Sr and 137Cs, Environ. Sci. Technol. 38 (2004) 850–857. https://doi.org/10.1021/ES0300463/ASSET/IMAGES/MEDIUM/ES0300463F00003.GIF.

[25] G. Steinhauser, V. Schauer, K. Shozugawa, Concentration of Strontium-90 at Selected Hot Spots in Japan, PLoS One 8 (2013). https://doi.org/10.1371/JOURNAL.PONE.0057760.

[26] D.J. Gunn, Mass transport phenomena : Christie J. Geankoplis, published by Holt, Rinehart and Winston, London, 1972, Chem. Eng. J. 5 (1973) 107–108. https://doi.org/10.1016/0300-9467(73)85014-2.

[27] H.W. Godbee, D.S. Joy, Assessment of the Loss of Radioactive Isotopes from Waste Solids to the Environment. Part 1: Background and Theory, Chem. Technol. Div. 8 (1974) 1–53.

[28] A.N.S. Nuclear, F. Standards, American National Standard Measurement of the Leachability of Solidified Low-Level Radioactive Wastes by a Short-Term Test Procedure, Am. Nucl. Soc. 2003 (2017).

[29] G.J. de Groot, H.A. van der Sloot, Determination of leaching characteristics of waste materials leading to environmental product certification, in: ASTM Spec. Tech. Publ., 1992: pp. 149–170. https://doi.org/10.1520/stp19548s.

[30] C. Pescatore, Leach rate expressions for performance assessment of solidified, low-level radioactive waste, Waste Manag. 11 (1991) 223–229. https://doi.org/10.1016/0956-053X(91)90069-H.

[31] O. Onuaguluchi, N. Banthia, S. Jain, Leaching of concrete with mine tailings, LTD, 2022. https://doi.org/10.1016/B978-0-12-824533-0.00010-4.

[32] ASTM C1308-21, Standard test method for accelerated leach test for measuring contaminant releases from solidified waste, ASTM Int. West Conshohocken, PA i (2021) 1–12. https://doi.org/10.1520/C1308-21.2.

[33] M.I. Ojovan, W.E. Lee, S.N. Kalmykov, Immobilisation of Radioactive Waste in Cement, 2019.

https://doi.org/10.1016/b978-0-08-102702-8.00017-0.

[34] F. Glasser, Application of inorganic cements to the conditioning and immobilisation of radioactive wastes, Handb. Adv. Radioact. Waste Cond. Technol. (2011) 67–135. https://doi.org/10.1533/9780857090959.1.67.

[35] Price of Cement - United States | IBISWorld, (2023). https://www.ibisworld.com/us/bed/price-of-cement/190/.

[36] G. Bar-Nes, Y. Peled, Z. Shamish, A. Katz, Cesium and strontium immobilization in portland cement pastes blended with pozzolanic additives, J. Nucl. Eng. Radiat. Sci. 3 (2017). https://doi.org/10.1115/1.4035415/369978.

[37] M. Atkins, F.P. Glasser, Application of portland cement-based materials to radioactive waste immobilization, Waste Manag. 12 (1992) 105–131. https://doi.org/10.1016/0956-053X(92)90044-J.

[38] N.D.M. Evans, Binding mechanisms of radionuclides to cement, Cem. Concr. Res. 38 (2008) 543–553. https://doi.org/10.1016/j.cemconres.2007.11.004.

[39] X. Ke, S.A. Bernal, T. Sato, J.L. Provis, Alkali aluminosilicate geopolymers as binders to encapsulate strontium-selective titanate ion-exchangers, Dalt. Trans. 48 (2019) 12116–12126. https://doi.org/10.1039/C9DT02108F.

[40] IAEA, Long term behaviour of low and intermediate level waste packages under repository conditions, Long Term Behav. Low Intermed. Lev. Waste Packag. under Repos. Cond. (2004) 1–236. https://www.iaea.org/publications/6978/long-term-behaviour-of-low-and-intermediate-level-waste-packages-under-repository-conditions.

[41] IAEA, The Behaviours of Cementitious Materials in Long Term Storage and Disposal of Radioactive Waste, 2013. https://www.iaea.org/publications/10439/the-behaviours-of-cementitious-materials-in-long-term-storage-and-disposal-of-radioactive-waste.

[42] E.A. Tyupina, P.P. Kozlov, V.V. Krupskaya, Application of Cement-Based Materials as a Component of an Engineered Barrier System at Geological Disposal Facilities for Radioactive Waste—A Review, Energies 16 (2023). https://doi.org/10.3390/EN16020605.

[43] K.G. Papadokostaki, A. Savidou, Study of leaching mechanisms of caesium ions incorporated in Ordinary Portland Cement, J. Hazard. Mater. 171 (2009) 1024–1031. https://doi.org/10.1016/j.jhazmat.2009.06.118.

[44] S. Goñi, A. Guerrero, M.P. Lorenzo, Efficiency of fly ash belite cement and zeolite matrices for immobilizing cesium, J. Hazard. Mater. 137 (2006) 1608–1617. https://doi.org/10.1016/J.JHAZMAT.2006.04.059.

[45] A. Guerrero, M.S. Hernández, S. Goñi, Cemented materials in the LLW and MLW spanish disposal, Mater. Construcción 1999 (1999) 31–40. http://www.scopus.com/scopus/inward/record.url?eid=2-s2.0-0347769786&partnerID=40&rel=R6.5.0.

[46] Environment Canada, Proposed evaluation protocol for cement-based solidified wastes, Environ. Prot. Ser. 178; EPS 3 (1991) 45.

[47] X. Xu, H. Bi, Y. Yu, X. Fu, S. Wang, Y. Liu, P. Hou, X. Cheng, Low leaching characteristics and encapsulation mechanism of Cs+ and Sr2+ from SAC matrix with radioactive IER, J. Nucl. Mater. 544

(2021) 152701. https://doi.org/10.1016/J.JNUCMAT.2020.152701.

[48] J.Y. Pyo, W. Um, J. Heo, Magnesium potassium phosphate cements to immobilize radioactive concrete wastes generated by decommissioning of nuclear power plants, Nucl. Eng. Technol. 53 (2021) 2261–2267. https://doi.org/10.1016/J.NET.2021.01.005.

[49] J.G. Jang, S.M. Park, H.K. Lee, Physical barrier effect of geopolymeric waste form on diffusivity of cesium and strontium, J. Hazard. Mater. 318 (2016) 339–346. https://doi.org/10.1016/j.jhazmat.2016.07.003.

[50] H.M. Johnston, D.J. Wilmot, Sorption and diffusion studies in cementitious grouts, Waste Manag. 12 (1992) 289–297. https://doi.org/10.1016/0956-053X(92)90055-N.

[51] M.I. Ojovan, W.E. Lee, S.N. Kalmykov, Performance of Wasteform Materials, An Introd. to Nucl. Waste Immobil. (2019) 433–461. https://doi.org/10.1016/b978-0-08-102702-8.00023-6.

[52] J.Y. Goo, B.J. Kim, M. Kang, J. Jeong, H.Y. Jo, J.S. Kwon, Leaching Behavior of Cesium, Strontium, Cobalt, and Europium from Immobilized Cement Matrix, Appl. Sci. 2021, Vol. 11, Page 8418 11 (2021) 8418. https://doi.org/10.3390/APP11188418.

[53] F.P. Glasser, Fundamental aspects of cement solidification and stabilisation, J. Hazard. Mater. 52 (1997) 151–170. https://doi.org/10.1016/S0304-3894(96)01805-5.

[54] J.J. Thomas, J.J. Chen, A.J. Allen, H.M. Jennings, Effects of Decalcification on the Microstructure and Surface Area of Cement and Tricalcium Silicate Pastes, 34 (2004) 2297–2307. https://doi.org/10.1016/j.cemconres.2004.04.007.

[55] J. Jdaini, C. Cau Dit Coumes, Y. Barré, M.-N. De Noirfontaine, M. Courtial, E. Garcia-Caurel, F. Dunstetter, C. Cau, D. Coumes, M. Cour-Tial, D. Gorse-Pomonti, Strontium release from wollastonite-based brushite cement paste under semi-dynamic leaching conditions, (2022). https://cnrs.hal.science/hal-03776320 (accessed May 25, 2023).

[56] M.W. Barnes, B.E. Scheetz, L.D. Wakeley, S.D. Atkinson, D.M. Roy, Stability of I and SR Radiophases in Cement Matrices, MRS Proc. 6 (1981) 147. https://doi.org/10.1557/PROC-6-147.

[57] H. Matsuzuru, A. Ito, Leaching behaviour of strontium-90 in cement composites, Ann. Nucl. Energy 4 (1977) 465–470. https://doi.org/10.1016/0306-4549(77)90020-2.

[58] Q. Li, Z. Sun, D. Tao, Y. Xu, P. Li, H. Cui, J. Zhai, Immobilization of simulated radionuclide 133Cs+by fly ash-based geopolymer, J. Hazard. Mater. 262 (2013) 325–331. https://doi.org/10.1016/j.jhazmat.2013.08.049.

[59] N.B. Singh, B. Middendorf, Geopolymers as an alternative to Portland cement: An overview, Constr. Build. Mater. 237 (2020). https://doi.org/10.1016/J.CONBUILDMAT.2019.117455.

[60] A. Cleetus, R. Shibu, V.K. Paul, B. Jacob, Analysis and Study of the Effect of GGBFS on Concrete Structures, Irjet 5 (2018) 3033–3037. https://www.academia.edu/download/56787295/IRJET-V5I3716.pdf (accessed March 15, 2022).

[61] R.M. Andrew, Global CO2 emissions from cement production, 1928-2018, Earth Syst. Sci. Data 11 (2019) 1675–1710. https://doi.org/10.5194/ESSD-11-1675-2019.

[62] I. Chang, M. Lee, G.C. Cho, Global CO2 Emission-Related Geotechnical Engineering Hazards and the

Mission for Sustainable Geotechnical Engineering, Energies 2019, Vol. 12, Page 2567 12 (2019) 2567. https://doi.org/10.3390/EN12132567.

[63] G.A. Khoury, Compressive strength of concrete at high temperatures: A reassessment, Mag. Concr. Res. 44 (1992) 291–309. https://doi.org/10.1680/macr.1992.44.161.291.

[64] T. Bakharev, Resistance of geopolymer materials to acid attack, Cem. Concr. Res. 35 (2005) 658–670. https://doi.org/10.1016/J.CEMCONRES.2004.06.005.

[65] P. Bouniol, Contribution of the Tricalcium Silicate Hydration Products to the Formation of Radiolytic H 2 : A Systemic Approach, J. Adv. Concr. Technol. 20 (2022) 72–84. https://doi.org/10.3151/jact.20.72.

[66] A.J. Klemm, M. Wieloch, P. Klemm, W. Marks, Multicriterion optimisation approach in a design of cementitious composites with improved resistance to freezing/thawing, in: High Perform. Struct. Mater., 2004: pp. 579–587. https://www.witpress.com/elibrary/wit-transactions-on-the-built-environment/76/14019 (accessed March 11, 2022).

[67] Z. Xu, Z. Jiang, D. Wu, X. Peng, Y. Xu, N. Li, Y. Qi, P. Li, Immobilization of strontium-loaded zeolite A by metakaolin based-geopolymer, Ceram. Int. 43 (2017) 4434–4439. https://doi.org/10.1016/j.ceramint.2016.12.092.

[68] S. Pareek, Y. Suzuki, K. ichi Kimura, Y. Fujikura, Y. Araki, Radiation shielding properties and freeze-thaw durability of high-density concrete for storage of radioactive contaminated soil in Fukushima, Ageing Mater. Struct. Towar. Sci. Solut. Ageing Our Assets (2017) 97–109. https://doi.org/10.1007/978-3-319-70194-3_8.

[69] C. Shi, A. Fernández-Jiménez, Stabilization/solidification of hazardous and radioactive wastes with alkali-activated cements, J. Hazard. Mater. 137 (2006) 1656–1663. https://doi.org/10.1016/j.jhazmat.2006.05.008.

[70] Z. Ji, Y. Pei, Bibliographic and visualized analysis of geopolymer research and its application in heavy metal immobilization: A review, J. Environ. Manage. 231 (2019) 256–267. https://doi.org/10.1016/j.jenvman.2018.10.041.

[71] S.A. Rasaki, Z. Bingxue, R. Guarecuco, T. Thomas, Y. Minghui, Geopolymer for use in heavy metals adsorption, and advanced oxidative processes: A critical review, J. Clean. Prod. 213 (2019) 42–58. https://doi.org/10.1016/j.jclepro.2018.12.145.

[72] Y. Zhu, Z. Zheng, Y. Deng, C. Shi, Z. Zhang, Advances in immobilization of radionuclide wastes by alkali activated cement and related materials, Cem. Concr. Compos. 126 (2022) 104377. https://doi.org/10.1016/J.CEMCONCOMP.2021.104377.

[73] T.H. Vu, N. Gowripalan, Mechanisms of Heavy Metal Immobilisation using Geopolymerisation Techniques – A review, J. Adv. Concr. Technol. 16 (2018) 124–135. https://doi.org/10.3151/jact.16.124.

[74] J. Davidovits, Geopolymers - Inorganic polymeric new materials, J. Therm. Anal. 37 (1991) 1633–1656. https://doi.org/10.1007/BF01912193.

[75] J.L. Provis, J.S.J. Van Deventer, Geopolymers: Structures, processing, properties and industrial applications, Elsevier Ltd, 2009. https://doi.org/10.1533/9781845696382.

[76] J.L. Provis, Immobilisation of toxic wastes in geopolymers, Geopolymers (2009) 421–440. https://doi.org/10.1533/9781845696382.3.421.

[77] S. Fu, P. He, M. Wang, J. Cui, M. Wang, X. Duan, Z. Yang, D. Jia, Y. Zhou, Hydrothermal synthesis of pollucite from metakaolin-based geopolymer for hazardous wastes storage, J. Clean. Prod. 248 (2020) 119240. https://doi.org/10.1016/j.jclepro.2019.119240.

[78] P. He, R. Wang, S. Fu, M. Wang, D. Cai, G. Ma, M. Wang, J. Yuan, Z. Yang, X. Duan, Y. Wang, D. Jia, Y. Zhou, Safe trapping of cesium into doping-enhanced pollucite structure by geopolymer precursor technique, J. Hazard. Mater. 367 (2019) 577–588. https://doi.org/10.1016/j.jhazmat.2019.01.013.

[79] S. Jain, N. Banthia, T. Troczynski, Conditioning of simulated cesium radionuclides in NaOH-activated fly ash-based geopolymers, J. Clean. Prod. 380 (2022) 134984. https://doi.org/10.1016/j.jclepro.2022.134984.

[80] M. Arbel Haddad, E. Ofer-Rozovsky, G. Bar-Nes, E.J.C. Borojovich, A. Nikolski, D. Mogiliansky, A. Katz, Formation of zeolites in metakaolin-based geopolymers and their potential application for Cs immobilization, J. Nucl. Mater. 493 (2017) 168–179. https://doi.org/10.1016/J.JNUCMAT.2017.05.046.

[81] S. Jain, N. Banthia, T. Troczynski, Leaching of immobilized cesium from NaOH-activated fly ash-based geopolymers, Cem. Concr. Compos. 133 (2022) 104679. https://doi.org/10.1016/j.cemconcomp.2022.104679.

[82] S. Jain, S. Roy, N. Banthia, T. Troczynski, Kinetics of in-situ pollucite crystallization in relation to cesium immobilization in the fly ash-based geopolymers, J. Mater. Sci. 58 (2023) 9908–9922. https://doi.org/10.1007/S10853-023-08653-7/METRICS.

[83] M. Komljenović, G. Tanasijević, N. Džunuzović, J.L. Provis, Immobilization of cesium with alkali-activated blast furnace slag, J. Hazard. Mater. 388 (2020) 121765. https://doi.org/10.1016/J.JHAZMAT.2019.121765.

[84] N. Deng, H. An, H. Cui, Y. Pan, B. Wang, L. Mao, J. Zhai, Effects of gamma-ray irradiation on leaching of simulated 133Cs+ radionuclides from geopolymer wasteforms, J. Nucl. Mater. 459 (2015) 270–275. https://doi.org/10.1016/j.jnucmat.2015.01.052.

[85] A. Fernandez-Jimenez, D.E. MacPhee, E.E. Lachowski, A. Palomo, Immobilization of cesium in alkaline activated fly ash matrix, J. Nucl. Mater. 346 (2005) 185–193. https://doi.org/10.1016/j.jnucmat.2005.06.006.

[86] C. Kuenzel, J.F. Cisneros, T.P. Neville, L.J. Vandeperre, S.J.R. Simons, J. Bensted, C.R. Cheeseman, Encapsulation of Cs/Sr contaminated clinoptilolite in geopolymers produced from metakaolin, J. Nucl. Mater. 466 (2015) 94–99. https://doi.org/10.1016/J.JNUCMAT.2015.07.034.

[87] J. Tits, E. Wieland, C.J. Müller, C. Landesman, M.H. Bradbury, Strontium binding by calcium silicate hydrates, J. Colloid Interface Sci. 300 (2006) 78–87. https://doi.org/10.1016/j.jcis.2006.03.043.

[88] Q. Tian, K. Sasaki, Application of fly ash-based geopolymer for removal of cesium, strontium and arsenate from aqueous solutions: kinetic, equilibrium and mechanism analysis., Water Sci. Technol. a J. Int. Assoc. Water Pollut. Res. 79 (2019) 2116–2125. https://doi.org/10.2166/wst.2019.209.

[89] L. Jia, P. He, D. Jia, S. Fu, M. Wang, M. Wang, X. Duan, Z. Yang, Y. Zhou, Immobilization behavior of Sr in geopolymer and its ceramic product, J. Am. Ceram. Soc. 103 (2020) 1372–1384. https://doi.org/10.1111/JACE.16811.

[90] B. Walkley, X. Ke, O.H. Hussein, S.A. Bernal, J.L. Provis, Incorporation of strontium and calcium in geopolymer gels, J. Hazard. Mater. 382 (2020). https://doi.org/10.1016/j.jhazmat.2019.121015.

[91] Z. Xu, Z. Jiang, D. Wu, X. Peng, Y. Xu, N. Li, Y. Qi, P. Li, Immobilization of strontium-loaded zeolite A by metakaolin based-geopolymer, Ceram. Int. 43 (2017) 4434–4439. https://doi.org/10.1016/j.ceramint.2016.12.092.

[92] X. Liu, Y. Ding, X. Lu, Immobilization of simulated radionuclide 90Sr by fly ash-slag-metakaolin-based geopolymer, Nucl. Technol. 198 (2017) 64–69. https://doi.org/10.1080/00295450.2017.1292810.

[93] Q. Tian, K. Sasaki, Structural characterizations of fly ash-based geopolymer after adsorption of various metal ions, Environ. Technol. (United Kingdom) 42 (2021) 941–951. https://doi.org/10.1080/09593330.2019.1649469.

[94] N. Vandevenne, R.I. Iacobescu, Y. Pontikes, R. Carleer, E. Thijssen, K. Gijbels, S. Schreurs, W. Schroeyers, Incorporating Cs and Sr into blast furnace slag inorganic polymers and their effect on matrix properties, J. Nucl. Mater. 503 (2018) 1–12. https://doi.org/10.1016/j.jnucmat.2018.02.023.

[95] Q. Guangren, L. Yuxiang, Y. Facheng, S. Rongming, Improvement of metakaolin on radioactive Sr and Cs immobilization of alkali-activated slag matrix, J. Hazard. Mater. 92 (2002) 289–300. https://doi.org/10.1016/S0304-3894(02)00022-5.

[96] T. Huang, D. Song, L.X. Yin, S.W. Zhang, L.F. Liu, L. Zhou, Microwave irradiation assisted sodium hexametaphosphate modification on the alkali-activated blast furnace slag for enhancing immobilization of strontium, Chemosphere 241 (2020). https://doi.org/10.1016/j.chemosphere.2019.125069.

[97] P. He, J. Cui, M. Wang, S. Fu, H. Yang, C. Sun, X. Duan, Z. Yang, D. Jia, Y. Zhou, Interplay between storage temperature, medium and leaching kinetics of hazardous wastes in Metakaolin-based geopolymer, J. Hazard. Mater. 384 (2020). https://doi.org/10.1016/j.jhazmat.2019.121377.

[98] H. Lei, Y. Muhammad, K. Wang, M. Yi, C. He, Y. Wei, T. Fujita, Facile fabrication of metakaolin/slag-based zeolite microspheres (M/SZMs) geopolymer for the efficient remediation of Cs+ and Sr2+ from aqueous media, J. Hazard. Mater. 406 (2021). https://doi.org/10.1016/j.jhazmat.2020.124292.

[99] L. Li, Z. Xu, H. Li, J. Li, D. Hu, Y. Xiang, L. Han, X. Peng, Immobilization of strontium and cesium by aluminosilicate ceramics derived from metakaolin geopolymer-zeolite A composites via 1100 °C heating treatment, Ceram. Int. 48 (2022) 15236–15242. https://doi.org/10.1016/j.ceramint.2022.02.054.

[100] J.L. Provis, A. Palomo, C. Shi, Advances in understanding alkali-activated materials, Cem. Concr. Res. 78 (2015) 110–125. https://doi.org/10.1016/j.cemconres.2015.04.013.

[101] M.G. Blackford, J. V. Hanna, K.J. Pike, E.R. Vance, D.S. Perera, Transmission electron microscopy and nuclear magnetic resonance studies of geopolymers for radioactive waste immobilization, J. Am. Ceram. Soc. 90 (2007) 1193–1199. https://doi.org/10.1111/J.1551-2916.2007.01532.X.

[102] R.I. Chaerun, N. Soonthornwiphat, K. Toda, K. Kuroda, X. Niu, R. Kikuchi, T. Otake, Y. Elakneswaran, J.L. Provis, T. Sato, Retention mechanism of cesium in chabazite embedded into metakaolin-based alkali activated materials, J. Hazard. Mater. 440 (2022). https://doi.org/10.1016/j.jhazmat.2022.129732.

[103] J. Ryu, S. Kim, H.-J. Hong, J. Hong, Strontium ion (Sr2) separation from seawater by hydrothermally structured titanate nanotubes: Removal vs. recovery, Chem. Eng. J. 304 (11AD) 503–510. https://doi.org/10.1016/j.cej.2016.06.131.

[104] E.M. Gartner, D.E. MacPhee, A physico-chemical basis for novel cementitious binders, Cem. Concr. Res. 41 (2011) 736–749. https://doi.org/10.1016/J.CEMCONRES.2011.03.006.

[105] H.A. Van Der Sloot, J.C.L. Meeussen, A.C. Garrabrants, D.S. Kosson, Review of the physical and chemical aspects of leaching assessment, Energy Res. Cent. Netherlands (2009).

[106] M. Fuhrmann, R. Pietrzak, J. Heiser, E.-M. Franz, P. Colombo, The Effects of Temperature on the Leaching Behavior of Cement Waste Forms - The Cement/Sodium Sulfate System, MRS Proc. 176 (1989) 75–80. https://doi.org/10.1557/PROC-176-75/METRICS.

[107] M. Erdemoğlu, M. Canbazoğlu, The leaching of SrS with water and the precipitation of SrCO3 from leach solution by different carbonating agents, Hydrometallurgy 49 (1998) 135–150. https://doi.org/10.1016/S0304-386X(98)00018-8.

[108] Z. Xu, Z. Jiang, D. Wu, X. Peng, Y. Xu, N. Li, Y. Qi, P. Li, Immobilization of strontium-loaded zeolite A by metakaolin based-geopolymer, Ceram. Int. 43 (2017) 4434–4439. https://doi.org/10.1016/J.CERAMINT.2016.12.092.

[109] Q. Tan, N. Li, Z. Xu, X. Chen, X. Peng, Q. Shuai, Z. Yao, Comparative performance of cement and metakaolin based-geopolymer blocks for strontium immobilization, J. Ceram. Soc. Japan 127 (2019) 44–49. https://doi.org/10.2109/JCERSJ2.18130.

[110] Y. Li, X. Peng, X. Jiang, R. An, L. Li, J. Li, H. Li, Z. Xu, Influence of freeze-thaw cycles and high temperature exposure on immobilization performance of geopolymer-zeolite A composites for strontium radionuclide, J. Radioanal. Nucl. Chem. 327 (2021) 1037–1043. https://doi.org/10.1007/S10967-020-07574-Y.

[111] R. Dayal, E.J. Readson, Cement-based engineered barriers for carbon-14 isolation, Waste Manag. 12 (1992) 189–200. https://doi.org/10.1016/0956-053X(92)90048-N.

[112] Y.F. Houst, F.H. Wittmann, Influence of porosity and water content on the diffusivity of CO2 and O2 through hydrated cement paste, Cem. Concr. Res. 24 (1994) 1165–1176. https://doi.org/10.1016/0008-8846(94)90040-X.

[113] T. Van Gerven, G. Cornelis, E. Vandoren, C. Vandecasteele, Effects of carbonation and leaching on porosity in cement-bound waste, Waste Manag. 27 (2007) 977–985. https://doi.org/10.1016/J.WASMAN.2006.05.008.

[114] Q. Chen, Y. Ke, L. Zhang, M. Tyrer, C.D. Hills, G. Xue, Application of accelerated carbonation with a combination of Na2CO3 and CO2 in cement-based solidification/stabilization of heavy metal-bearing sediment, J. Hazard. Mater. 166 (2009) 421–427. https://doi.org/10.1016/J.JHAZMAT.2008.11.067.

[115] B. Pandey, S.D. Kinrade, L.J.J. Catalan, Effects of carbonation on the leachability and compressive strength of cement-solidified and geopolymer-solidified synthetic metal wastes, J. Environ. Manage. 101 (2012) 59–67. https://doi.org/10.1016/J.JENVMAN.2012.01.029.

[116] M. Palacios, F. Puertas, Effect of carbonation on alkali-activated slag paste, J. Am. Ceram. Soc. 89 (2006) 3211–3221. https://doi.org/10.1111/J.1551-2916.2006.01214.X.

[117] S.M. Park, J.G. Jang, Carbonation-induced weathering effect on cesium retention of cement paste, J. Nucl.

Mater. 505 (2018) 159–164. https://doi.org/10.1016/J.JNUCMAT.2018.04.015.

[118] J.C. Walton, S. Bin-Shafique, R.W. Smith, N. Gutierrez, A. Tarquin, Role of Carbonation in Transient Leaching of Cementitious Wasteforms, Environ. Sci. Technol. 31 (1997) 2345–2349. https://doi.org/10.1021/ES960964J.

[119] M.S. Bin Shafique, J.C. Walton, N. Gutierrez, R.W. Smith, A.J. Tarquin, Influence of Carbonation on Leaching of Cementitious Wasteforms, J. Environ. Eng. 124 (1998) 463–467. https://doi.org/10.1061/(ASCE)0733-9372(1998)124:5(463).

[120] G. Bar-Nes, O. Klein-BenDavid, L. Chomat, N. Macé, M. Arbel-Haddad, S. Poyet, Sr immobilization in irradiated Portland cement paste exposed to carbonation, Cem. Concr. Res. 107 (2018) 152–162. https://doi.org/10.1016/J.CEMCONRES.2018.02.015.

[121] M.A. Venhuis, E.J. Reardon, M.A. Venhuis, Carbonation of cementitious wasteforms under supercritical and high pressure subcritical conditions, Environ. Technol. 24 (2003) 877–887. https://doi.org/10.1080/09593330309385624.

[122] J.L. Tanasijevic, J. Provis, V.N. Carevic, I.S. Ignjatovic, M.M. Komljenovic, EFFECT OF ACCELERATED CARBONATION ON THE EFFICIENCY OF EFFECT OF ACCELERATED CARBONATION ON THE EFFICIENCY OF IMMOBILIZATION OF Cs IN THE ALKALI-, in: CoMS_2020, Slovenian National Building and Civil Engineering Institute (ZAG), 2021: p. 304. https://grafar.grf.bg.ac.rs/handle/123456789/2270 (accessed January 23, 2024).

[123] S.B. Yarusova, O.O. Shichalin, A.A. Belov, S.A. Azon, I.Y. Buravlev, A. V. Golub, V.Y. Mayorov, A. V. Gerasimenko, E.K. Papynov, A.I. Ivanets, A.A. Buravleva, E.B. Merkulov, V.A. Nepomnyushchaya, O. V. Kapustina, P.S. Gordienko, Synthesis of amorphous KAlSi3O8 for cesium radionuclide immobilization into solid matrices using spark plasma sintering technique, Ceram. Int. 48 (2022) 3808–3817. https://doi.org/10.1016/J.CERAMINT.2021.10.164.

[124] O.O. Shichalin, A.A. Belov, A.P. Zavyalov, E.K. Papynov, S.A. Azon, A.N. Fedorets, I.Y. Buravlev, M.I. Balanov, I.G. Tananaev, Y. Shi, Q. Zhang, M. Niu, W. Liu, A.S. Portnyagin, Reaction synthesis of SrTiO3 mineral-like ceramics for strontium-90 immobilization via additional in-situ synchrotron studies, Ceram. Int. 48 (2022) 19597–19605. https://doi.org/10.1016/J.CERAMINT.2022.03.068.

[125] J. Jang, S. Park, H. Lee, Cesium and Strontium Retentions Governed by Aluminosilicate Gel in Alkali-Activated Cements, Materials (Basel). 10 (2017) 447. https://doi.org/10.3390/ma10040447.

[126] Q. Tian, S. Nakama, K. Sasaki, Immobilization of cesium in fly ash-silica fume based geopolymers with different Si/Al molar ratios, Sci. Total Environ. 687 (2019) 1127–1137. https://doi.org/10.1016/j.scitotenv.2019.06.095.

[127] C. Chlique, D. Lambertin, P. Antonucci, F. Frizon, P. Deniard, XRD analysis of the role of cesium in sodium-based geopolymer, J. Am. Ceram. Soc. 98 (2015) 1308–1313. https://doi.org/10.1111/jace.13399.

[128] J.L. Bell, P. Sarin, J.L. Provis, R.P. Haggerty, P.E. Driemeyer, P.J. Chupas, J.S.J. Van Deventer, W.M. Kriven, Atomic structure of a cesium aluminosilicate geopolymer: A pair distribution function study, Chem. Mater. 20 (2008) 4768–4776. https://doi.org/10.1021/cm703369s.

[129] L. Li, Z. Xu, H. Li, J. Li, D. Hu, Y. Xiang, L. Han, X. Peng, Immobilization of strontium and cesium by aluminosilicate ceramics derived from metakaolin geopolymer-zeolite A composites via 1100 °C heating treatment, Ceram. Int. 48 (2022) 15236–15242. https://doi.org/10.1016/J.CERAMINT.2022.02.054.

[130] A.S. Wagh, S.Y. Sayenko, V.A. Shkuropatenko, R. V. Tarasov, M.P. Dykiy, Y.O. Svitlychniy, V.D. Virych, Y.A. Ulybkina, Experimental study on cesium immobilization in struvite structures, J. Hazard. Mater. 302 (2016) 241–249. https://doi.org/10.1016/J.JHAZMAT.2015.09.049.